Design of an Ultraviolet Absorption Spectroscopy Oil Concentration Sensor for Online HVAC Measurements

by

Roman M. Luz III

B.S Mechanical Engineering
Massachusetts Institute of Technology, 2001

Submitted to the Department of Mechanical Engineering in Partial Fulfillment of the Requirements for the Degree of

Master of Science in Mechanical Engineering
at the
Massachusetts Institute of Technology

February 2005

Signature of Author: _____
Department of Mechanical Engineering
November 23, 2004

Certified by: _____
Haruhiko H. Asada
Professor of Mechanical Engineering
Thesis Supervisor

Accepted by: _____
Lallit Anand
Professor of Mechanical Engineering
Chairman, Department Committee on Graduate Students

Design of an Ultraviolet Absorption Spectroscopy Oil Concentration Sensor for Online HVAC Measurements

by

Roman M. Luz III

Submitted to the Department of Mechanical Engineering
on November 24, 2004 in Partial Fulfillment of the
Requirements for the Degree of Master of Science in
Mechanical Engineering

ABSTRACT

Recent advances in the modeling and control of the vapor compression cycle has developed the need for a real time oil concentration rate (OCR) sensor. Because of its ability to give the most accurate online measurements of OCR, ultraviolet absorption spectroscopy has been selected as the measurement approach. Related work in this field is based on models that are unable to make accurate measurements down to zero percent oil concentration. Because of the extremely low OCR of modern HVAC units, the operating range of the sensor must be zero to one percent oil concentration.

Improvements to prior models that employ Beer-Lambert's Law will allow the sensor to operate with improved accuracy over the entire operating range. This report details the design of the physical hardware, the analytical modeling, and the calibration methods to build and operate the OCR sensor.

Thesis Supervisor: Harry H. Asada

Title: Ford Professor of Mechanical Engineering

Table of Contents

Nomenclature

General Symbols

λ	wavelength (nm)
ε	extinction coefficient (m^{-1})
c	concentration ( )
l	optical pathlength (mm)
a	absorbance ( )
β	slope of absorbance Vs. pathlength (m^{-1})
I	light intensity ( )
T	transmission of light ( )
$S_{L,L}$	sample variance of pathlength (m^2)
$S_{A,L}$	sample covariance of absorbance and pathlength (m)
R^2	coefficient of determination
J	sum of squared errors to minimize in least squares estimation
w	weighting factor for a wavelength

Subscripts

m	index for wavelength, m = 1, 2, …, M
n	index for substrate or sample concentration, n = 1, 2, …, N
p	index for pathlength, p = 1, 2, …, P

Vectors and Matrices

L	[Px1] pathlength matrix, l_p
A_p	[NxM] absorbance matrix of $a_{m,n}$, for pathlength l_p
E	[2xM] extinction coefficient matrix of $\varepsilon_{m,n}$
C	[Nx2] concentration matrix of $c_{m,n}$
B	[NxM] slope matrix of $\beta_{m,n}$
W	[MxM] diagonal weighting matrix of w_m

1 Introduction: OCR sensors in HVAC systems

Air conditioning units contain two fluids that are crucial for proper operation of the refrigeration cycle – the refrigerant and the lubricant. The refrigerant is the working fluid that effectively transfers heat away from the load to provide cooling. Its thermal properties such as heat capacity, conductivity, and boiling temperature as well as its kinetic properties such as viscosity and density are critical parameters in the operation of the system. The image below shows a diagram of the refrigerant flow through an air conditioning cycle.

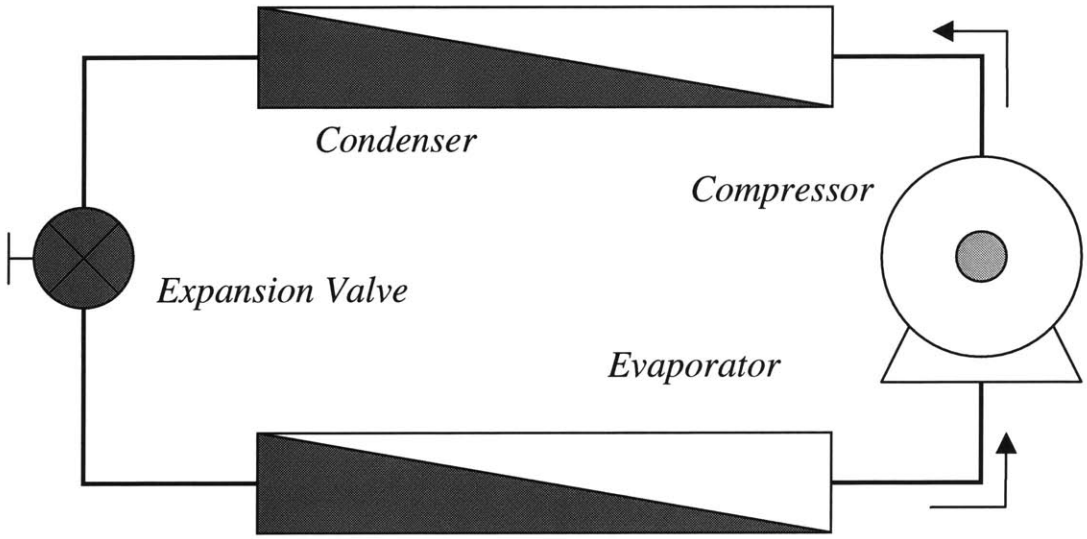

Figure 1: A generic HVAC circuit. The blue areas between the condenser and the evaporator are called the liquid line because the refrigerant should be fully liquid in these regions.

The less often considered fluid is the lubricant in the compressor. The compressor is practically the only moving part in the system; thus it is the only component that requires lubrication to reduce wear. The lubricant's high viscosity is the critical property that protects the compressor parts and reduces friction.

Ideally the lubricant and refrigerant would remain in the appropriate components in the system. But trace amounts of oil escape the workings of the compressor and drift into the refrigeration cycle. Likewise, the refrigerant has the potential to condense and mix with the volume of lubricant in the oil gallery at the basin of the compressor. Thus, the two fluids inevitably circulate throughout all components in the system. The accumulator and compressor are to locations that build up large amounts of mixed oil and refrigerant; their images are below.

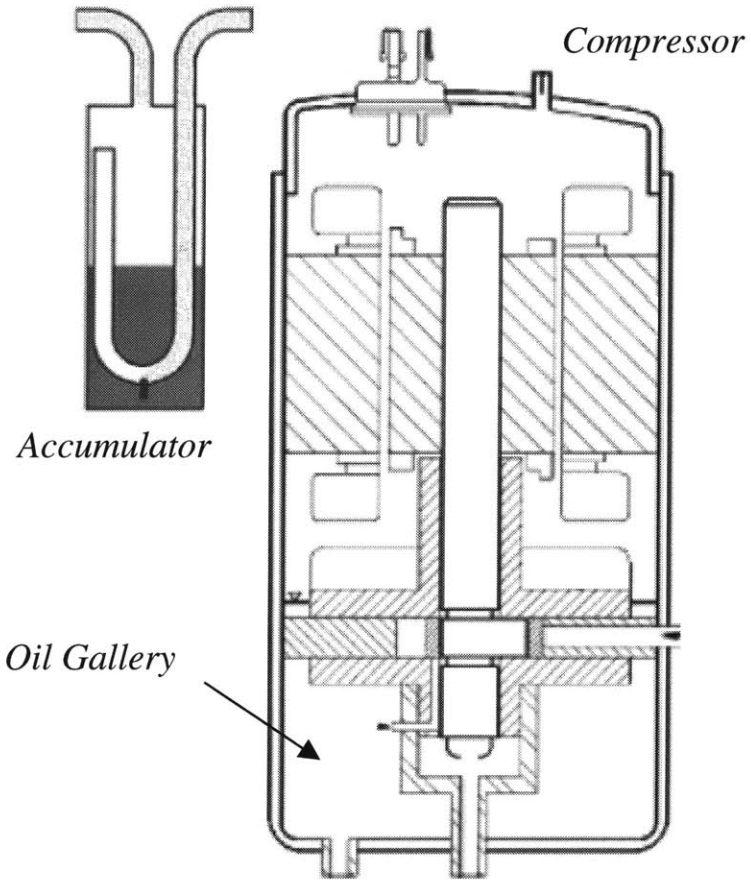

Figure 2: Images of the compressor and accumulator, two locations where the oil and refrigerant experience heavy mixing. These images are taken from [1].

The distribution of lubricant in the refrigeration cycle greatly affects the fluid properties and behaviors of the working fluid. The higher the oil concentration in the refrigerant, the more adversely the critical properties of the fluid will change. Therefore, the cooling capacity and efficiency of the unit will decrease as the oil circulation rate (OCR) increases. Likewise, as the refrigerant concentration in the oil reserve rises, the viscosity of the lubricant decreases. In extreme cases the compressor can overheat and damage itself due to wear. The disastrous scenario of an oil buildup in the intricate tubing of the heat exchangers and the valves may be avoided if the fluids mix rather than separate. As a result, air conditioner designers engineered the two fluids to be miscible so that oil cannot build up in the system's components.

Because the mixing of these fluids has a significant adverse effect on the system performance and reliability, engineers are currently modeling these intricacies of the refrigeration system. The critical fluid properties discussed above can be found as a function of the concentration of the oil-refrigerant mixture. Therefore the oil concentration throughout the system is an important input to a thermal-fluid model of a refrigeration unit. Observer models are also under construction that specifically track the distribution and circulation of oil throughout the system. In these models the OCR is the

output that will be supplied to the models previously mentioned. Thus, the OCR needs to be measured either to validate the observer models or to provide an input to the system models.

There are various techniques to measure oil concentration, but few are capable of measuring the dynamic oil circulation rate with great accuracy, especially the low concentrations found in today's HVAC units. Mass sampling, viscocity sensors, ultrasonic time of flight, and density measurements with corriolis meters are examples of such methods. In a comprehensive comparison of such methods by United Technologies Research Center [2], ultraviolet (UV) absorption spectroscopy was determined to be one of the most accurate techniques for the oils and hydrofluorocarbon (HFC) refrigerants used today. Absorption spectroscopy has the potential to take measurements during operation (inline measurements), has one of the best measurement ranges for low concentrations, and has the lowest uncertainty available today.

Related work has been applied to automobile air conditioners with higher OCR levels [4]. Their methodology will be used as a foundation for understanding more complex analysis. However, new techniques are necessary for measuring the extremely low oil concentrations found in industrial refrigeration units. The oil concentration in these units is an order of magnitude lower than those found in automobiles. Accurately measuring trace amounts of oil – down to zero percent – will be possible with modifications to the prior model.

The new model will take into account the absorption due to the refrigerant, which dominates the measurements at increasingly low oil concentrations. Noise reduction techniques will be applied to redundant measurements that utilize the full set of available data. This will statistically improve the measurements and make them more robust against noisy inputs.

The expertise gained from this work can lead to similar technologies that are capable of measuring high oil concentrations in the compressor oil gallery, the accumulator, or various other applications beyond the realm of HVAC.

2 Background: absorbance spectroscopy

2.1 Absorbance of light

Absorbance spectroscopy is used to identify the components of an unknown sample. In this procedure, light emitted from a reliable source is guided through an unknown mixture; then a spectrophotometer measures the light intensity before and after the light passes through the sample. This basic process is displayed in the diagram below.

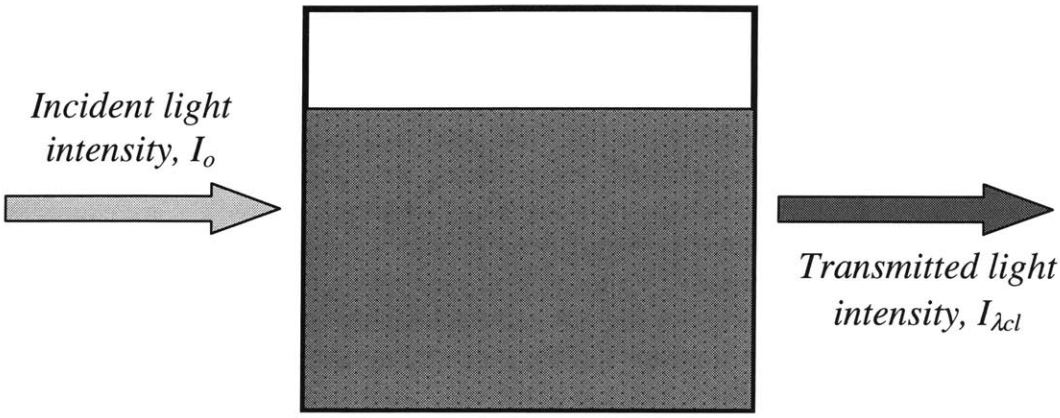

Figure 3: A schematic of light absorbance through a sample fluid.

In the diagram, the subscript λ refers to the wavelength of light, c refers to the concentration of a critical substrate in the mixture, and l refers to the optical pathlength through the sample. These are controlled parameters that characterize the optical properties of the substances being measured.

The incident light can be filtered so that the sample is only exposed to light with a narrow band of wavelengths. In this way, the sample's absorbance is measured as a function of wavelength to generate an absorbance spectrum. Light intensity is absorbed at higher levels when the frequency of the light is near the vibration frequency of the molecules in the sample [3]. As a result, the absorbance is highly dependent on the frequency of light and the substances in the mixture. The unique absorbance spectra of each component in an unknown mixture allow the concentrations of the components to be identified.

The absorbance, a, for a particular wavelength, λ, mixture of concentrations (by volume), c, and pathlength, l, is defined as

$$a_{\lambda cl} \equiv \log\left(\frac{I_0}{I_{\lambda cl}}\right) = -\log\left(T_{\lambda cl}\right), \tag{1}$$

where I is the light intensity, and T is the transmission of light. The base of the logarithm is inconsequential; base 10 is used in this report because the measurement instrument uses that value.

2.2 The Beer-Lambert Law

The Beer-Lambert Law models the relationship between the incident and exiting light intensity as it passes through a multi-substrate mixture. According to the model, the light intensity decreases exponentially with an increasing pathlength and increasing concentration of substrate. The equation below shows this relationship:

$$I_{\lambda cl} = I_o 10^{-\varepsilon_\lambda cl}. \tag{2}$$

The extinction coefficient, ε, is a property of the substrate and the wavelength of light. It is only determined experimentally. Using the definition of absorbance with Equation (2), Beer-Lambert's Law takes its usual form,

$$a_{\lambda cl} = \log\left(\frac{I_o}{I_{\lambda cl}}\right) = \varepsilon_\lambda cl. \tag{3}$$

This model predicts that the absorbance of light due to each substrate in the mixture varies linearly with concentration and pathlength for all wavelengths.

In general, multiple substrates will contribute to the absorbance of light. Expanding upon the model above, the total absorbance becomes the sum of each substrate's absorbance according to the following:

$$\begin{aligned} a_{\lambda cl} &= \varepsilon_{\lambda,1} c_1 l + \varepsilon_{\lambda,2} c_2 l + \ldots + \varepsilon_{\lambda,N} c_N l \\ &= l \sum_{n=1}^{N} \varepsilon_{\lambda,n} c_n \end{aligned}. \tag{4}$$

Equation (4) shows that if the pathlength goes to zero, the absorbance must be zero as well. Thus the y-intercept of the line formed when plotting absorbance against pathlength must be zero. The slope, β, of this line is an important parameter in characterizing a sample. β is defined below:

$$\begin{aligned} \beta_{\lambda c} &= \frac{d}{dl}(a_{\lambda cl}) \\ &= \sum_{n=1}^{N} \varepsilon_{\lambda,n} c_n \end{aligned}, \tag{5}$$

and it is clearly a function of the wavelength and the sample concentrations. The plot below shows measured data that demonstrates the linearity of the absorbance versus pathlength line and its slope.

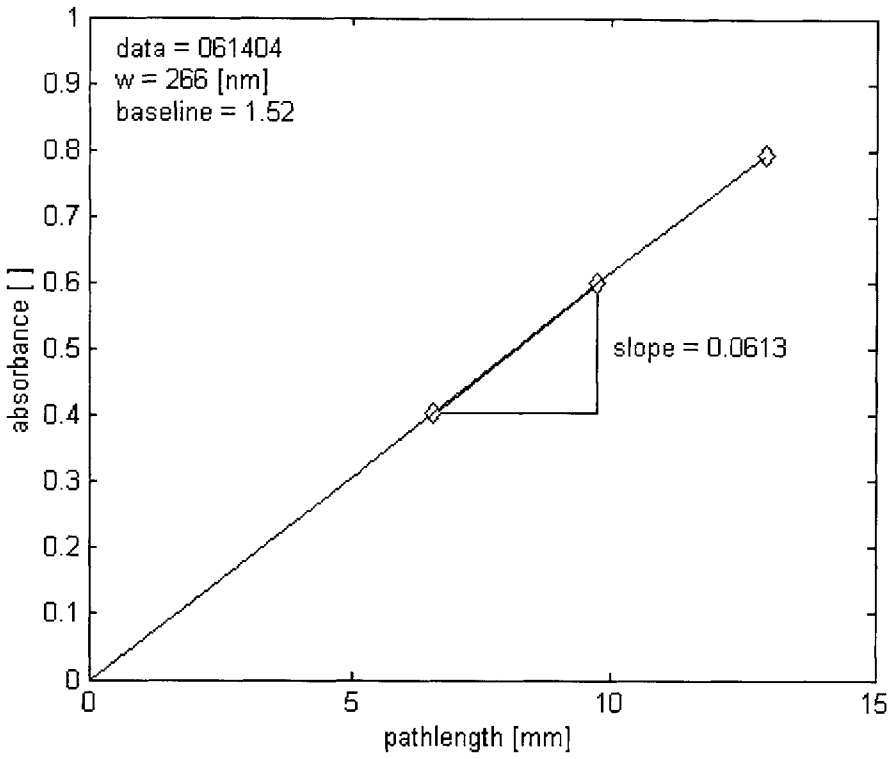

Figure 4: Ideal absorbance data is linear with pathlength and is zero at the origin

In the summation above, the subscript n represents the substrate in the sample, such as oil or refrigerant. The concentrations of each substrate must add to one, so the following constraint must hold:

$$\sum_{n=1}^{N} c_n = 1. \tag{6}$$

3 Applying spectroscopy to oil concentration sensors

The spectrophotometer is simply a device that supplies light intensity measurements through a sample. In order use this device as an oil concentration sensor, a calibration technique is necessary to interpret those measurements. The sections below discuss some concepts used in this interpretation.

3.1 Optimizing the wavelength band for the oil and refrigerant

Before the absorbance measurements can be made, the appropriate wavelength range of light must be chosen for the incident light. The electromagnetic spectrum is infinite and has been charted from gamma rays to radio waves. But spectroscopy applications typically use light in the ultraviolet and the infrared regions of the spectrum. For small oil concentrations in HFC refrigerants, a small range in the ultraviolet region around 265 nm has been identified as a location where the oil and refrigerant have desirable properties for an oil concentration sensor.

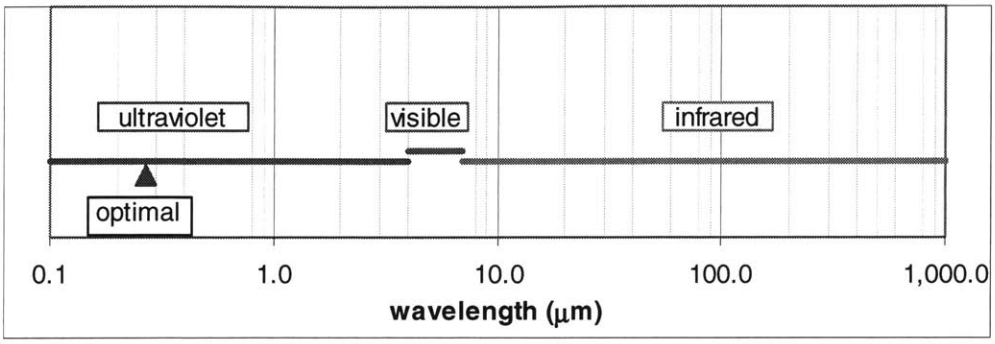

Figure 5: A plot showing the regions of the electromagnetic spectrum that are typical of spectroscopy applications. The optimal location for an oil concentration sensor is designated by the triangle in the ultraviolet region.

In this range the light absorbance is very sensitive to oil concentration and insensitive to refrigerant concentration. This implies that the extinction coefficient of the oil is vastly greater than that of the refrigerant at these wavelengths. Furthermore, the oil has a distinguishable absorbance spectrum whereas the refrigerant absorbance is not as responsive to changes in the wavelength of light. These distinguishable patterns aid in identifying an unknown mixture. The figure below shows the extinction coefficients of the oil and a refrigerant plotted against wavelength.

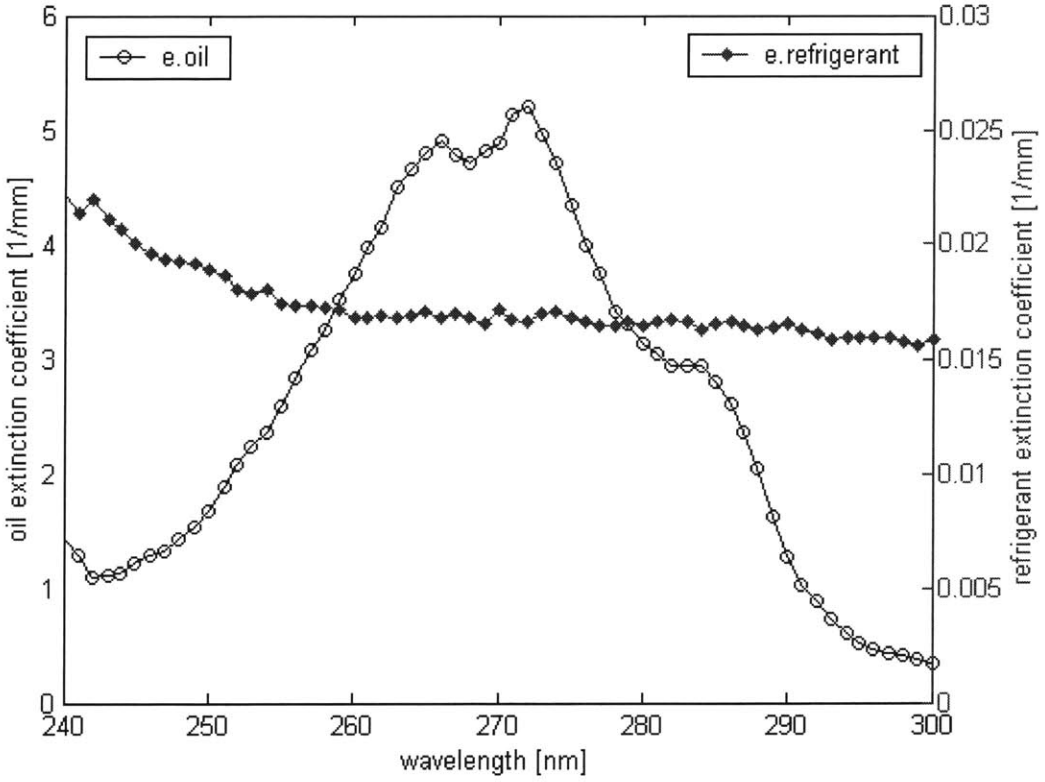

Figure 6: A plot of the estimations of the extinction coefficients of oil FVC50k (left axis) and isopropyl alcohol (right axis). The plot shows the unique spectra of these liquids and an order of magnitude difference in their values.

Notice that the oil is orders of magnitude more absorbent than the refrigerant at some wavelengths. The figure below shows the ratio of the extinction coefficients. The light is up to 300 times more sensitive to the presence of oil than it is to that of refrigerant at these wavelengths. These are some of the key features required to measure extremely low oil concentrations. Other performance measures regarding the selection and weighting of wavelengths will be discussed in the analysis section.

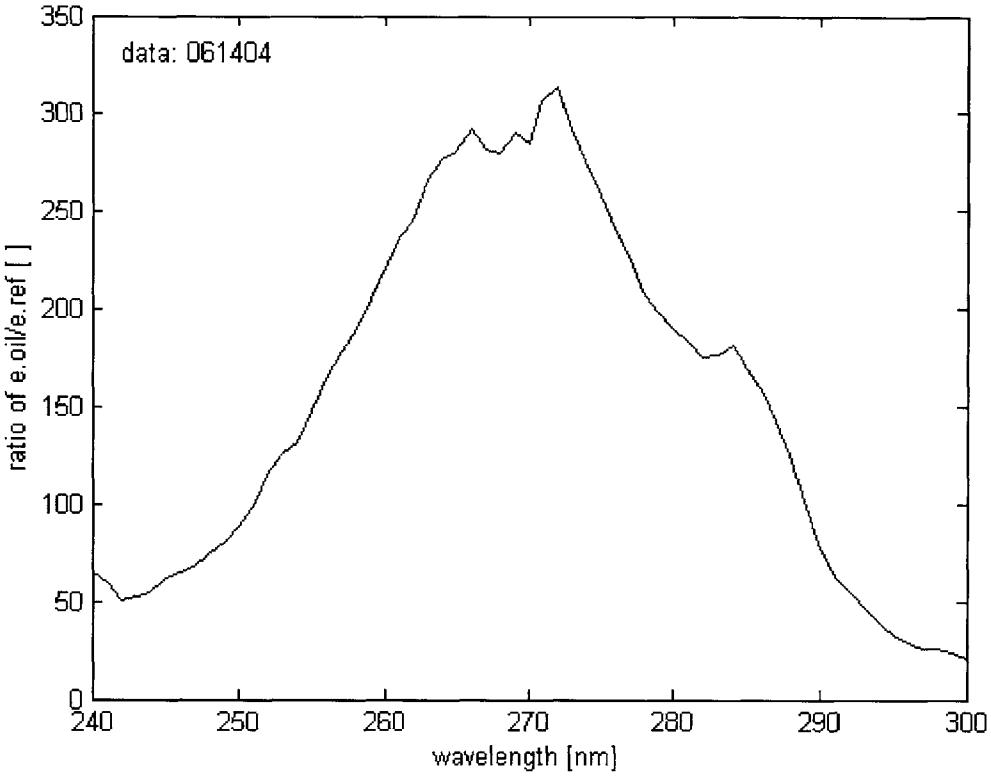

Figure 7: The ratio of the oil and refrigerant extinction coefficients determine the sensor's relative sensitivity to oil concentration as a function of wavelength.

Now the discussion of absorbance in general will be applied to a sample from an air conditioner with oil and refrigerant mixtures. For an HVAC oil concentration sensor, the sample has only two components in the mixture; thus the summation in Equation (4) can be expanded to two terms

$$a_{\lambda cl} = l\sum_{n=1}^{N} \varepsilon_{\lambda,n} c_n = l\left(\varepsilon_{\lambda,oil} c_{oil} + \varepsilon_{\lambda,refrigerant} c_{refrigerant}\right). \tag{7}$$

At the proper wavelengths and oil concentrations, the absorbance due to refrigerant may be low enough to justify neglecting it from the equation above. If the refrigerant is neglected, absorbance of the sample becomes

$$a_{\lambda cl} = \left(\varepsilon_{\lambda,oil} c_{oil}\right) l . \tag{8}$$

This assumption will be made in the following section, but will prove to be invalid at extremely low oil concentration levels.

3.2 Eliminating the baseline absorbance

When an absorbance measurement is performed, the ideal location to measure the incident and exiting light intensities would clearly be just before and just after the fluid samples. However, for many reasons this is impractical. First of all, some medium must guide the light from the sensors to the sample and back. Secondly, the sample must be enclosed in one way or another to hold it in place. This is especially true for pressurized refrigerants that vaporize at standard temperature and pressure. Therefore, there will always be a baseline absorbance created as the light travels through the optical network and through the various materials that guide it or hold the sample. Considering these losses, the measured absorbance, a^*, becomes the following:

$$\begin{aligned} a^*_{\lambda cl} &= a_{\lambda,baseline} + a_{\lambda cl} \\ &= a_{\lambda,baseline} + (\varepsilon_{\lambda,oil} c_{oil}) l \end{aligned} \quad . \tag{9}$$

Even with fiber optic cables to guide the light, the absorbance of the optics will have a significant dependence on wavelength in the deep UV range, as denoted above. Thus, the baseline absorbance, $a_{\lambda,baseline}$, must be characterized and corrected for in order to interpret the measurements.

The simplest method to eliminate the unwanted absorbance is to measure the absorbance of the optics separately and subtract from the measurements of the sample. The baseline absorbance can be estimated by removing the sample, closing the empty space that the sample occupied, and taking the measurement again. This is equivalent to a sample with zero pathlength. The second line in Equation (9) corroborates that a zero pathlength measurement should be equivalent to the baseline absorbance.

$$\begin{aligned} a^*_{\lambda cl_0} &= a_{\lambda,baseline} + (\varepsilon_{\lambda,oil} c_{oil}) 0 \\ &= a_{\lambda,baseline} \end{aligned} \quad . \tag{10}$$

this method will be referred to as the baseline method.

The procedure mentioned above can be thought of as a differential measurement with zero pathlength. In the operation below, the absorbance due to optics is cancelled in the subtraction. This result is attained using measurements at a pathlength l_1 and the theoretical zero pathlength, l_0.

$$\begin{aligned} a^*_{\lambda cl_1} - a^*_{\lambda cl_0} &= (a_{\lambda,baseline} + a_{\lambda cl_1}) - (a_{\lambda,baseline} + a_{\lambda cl_0}) \\ &= a_{\lambda cl_1} - a_{\lambda cl_0} = \varepsilon_{\lambda,oil} c_{oil} (l_1 - l_0) \\ &= \varepsilon_{\lambda,oil} c_{oil} l_1 \end{aligned} \quad . \tag{11}$$

However, it is difficult to set up the zero pathlength measurement to be consistent with the measurement from the enclosed sample. Furthermore, the enclosed sample and its fused silica windows have the tendency to change over time. The windows tend to collect a buildup on the inner surfaces, and this is the main cause of deterioration over time. The offline zero pathlength measurement is not likely to change in the same way as an installed sensor.

Therefore a better differential measurement is between two pathlengths of close proximity within the sample. This will yield the same result as Equation (11) before the zero pathlength is removed

$$a^*_{\lambda cl_2} - a^*_{\lambda cl_1} = \varepsilon_{\lambda,oil} c_{oil} (l_2 - l_1). \tag{12}$$

Dividing he known pathlengths from both sides of the equation above gives an equation of known terms on the left and unknown terms on the right:

$$\begin{aligned} \frac{a^*_{\lambda cl_2} - a^*_{\lambda cl_1}}{(l_2 - l_1)} &= \varepsilon_{\lambda,oil} c_{oil} \\ &= \beta_{\lambda c} \end{aligned} . \tag{13}$$

This method will be referred to as the differential method. These two measurements create a line in the absorbance-pathlength plane, and the measurements arranged on the left are an estimate of the slope of that line. But unlike Equation (5), this line will not pass through the origin. Rather the y-intercept (or zero pathlength) will have a value equal to the baseline absorbance.

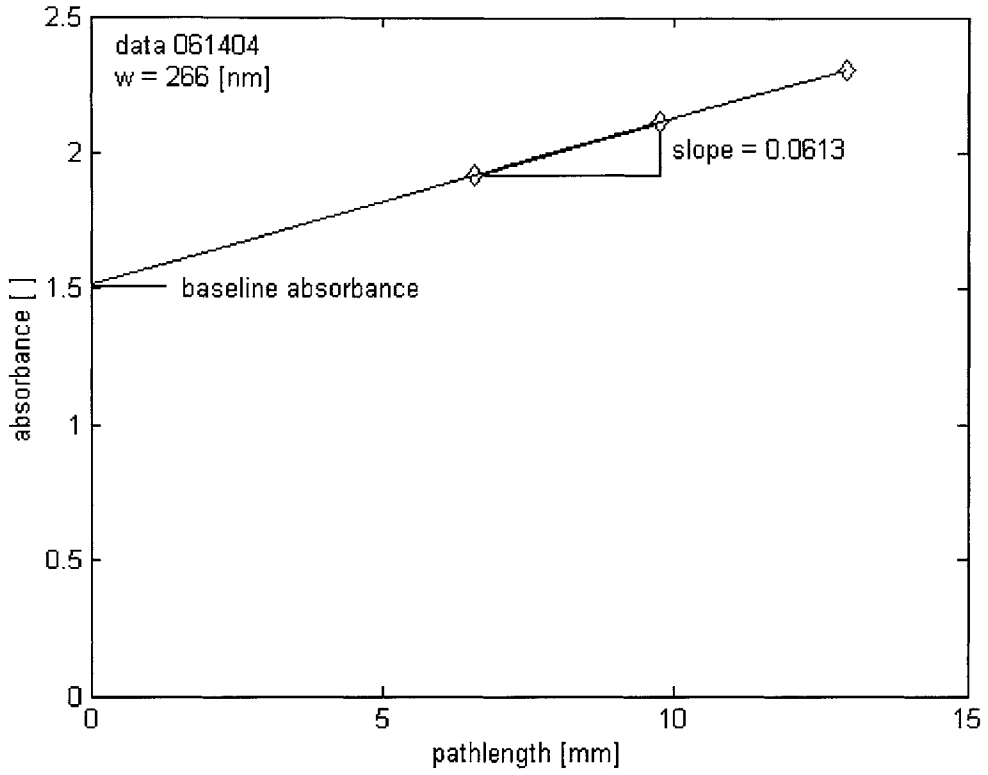

Figure 8: A plot of measured absorbance data has a baseline offset that needs to be corrected. The baseline absorbance is a function of wavelength, and this plot shows data at 266 nanometers.

Jasco Corporation and Nippondenso Ltd. [4] have developed a dual pathlength sensor that utilizes Equation (13) at an optimal wavelength. The calibration estimates the extinction coefficient at this singular wavelength in a sample of known oil concentration via the following expression:

$$\hat{\varepsilon}_{\lambda,oil} = \frac{a^*_{\lambda cl_2} - a^*_{\lambda cl_1}}{(l_2 - l_1)c_{oil}} = \frac{\beta_{\lambda c}}{c_{oil}}. \tag{14}$$

After $e_{\lambda,oil}$ is found, estimating the oil concentration in an unknown sample is just as straightforward:

$$\hat{c}_{oil} = \frac{a^*_{\lambda cl_2} - a^*_{\lambda cl_1}}{(l_2 - l_1)\hat{\varepsilon}_{\lambda,oil}} = \frac{\beta_{\lambda c}}{\hat{\varepsilon}_{\lambda,oil}}. \tag{15}$$

4 Utilizing the full model and measurements

The following sections will expand on the fundamental ideas presented above. These sections will describe an approach that uses the complete Beer-Lambert based model and the entire available data set – redundant pathlength and wavelength

measurements. The underlying concept is that utilizing more data will yield statistically improved sensor performance.

4.1 The low oil concentration effect

The assumption that the absorbance due to refrigerant is negligible was used to simplify the mathematics above. However, for a mixture with only two components, the math is manageable without this simplification. Furthermore, as the oil concentration approaches zero, the absorbance due to oil also approaches zero. Thus the absorbance due to the refrigerant dominates at extremely low oil concentrations. The absorbance due to the refrigerant will be shown to be increasingly significant as the oil concentration approaches zero. Therefore, if the sensor's working range should be as low as zero percent oil, then the refrigerant cannot be neglected.

The percent of absorbance due to the refrigerant can be calculated as a function of the oil concentration according to the Beer-Lambert Law shown in Equation (4). The plot below is made from a model using the peak oil extinction coefficient at a wavelength of 272 nm. Choosing this wavelength maximizes the oil absorbance and reduces the relative effect of the refrigerant.

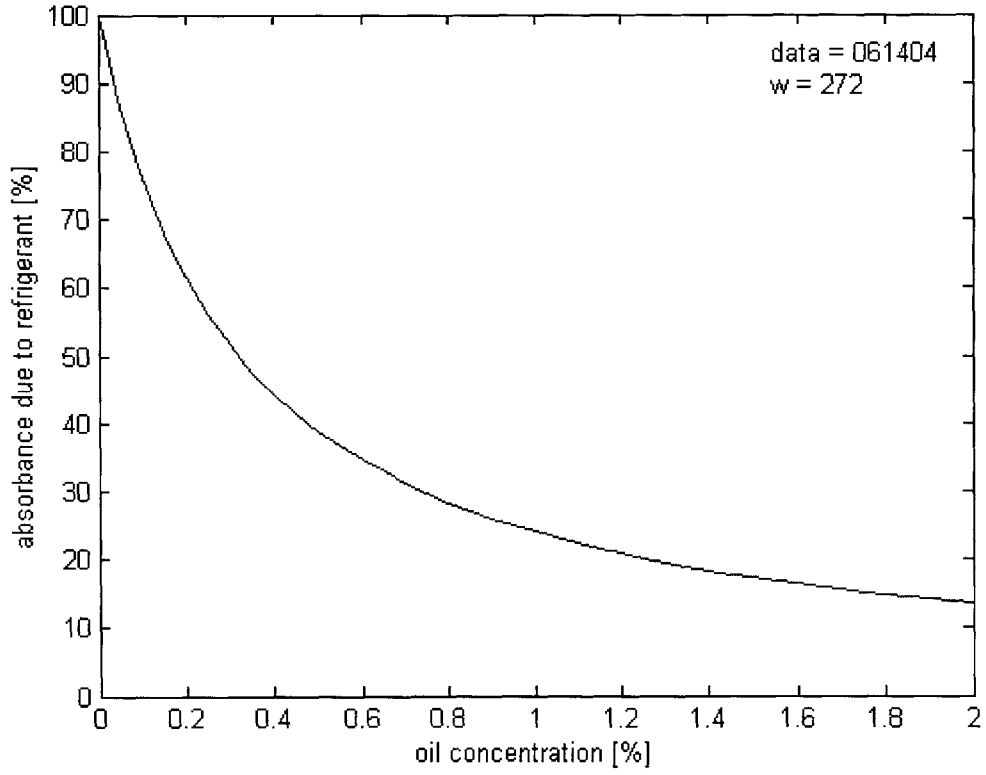

Figure 9: Output from a model of the absorbance due to the refrigerant at one wavelength. The absorbance due to the refrigerant becomes increasingly significant as the oil concentration approaches zero.

Even though the refrigerant's effect has been minimized at this wavelength, the refrigerant clearly has a significant effect for any oil concentration below 2%. From this

model we can see that at 0.5%, the typical oil concentration of an HVAC air conditioner, the refrigerant accounts for 40% of the absorbance. A more informative plot using actual data for multiple wavelengths is shown below:

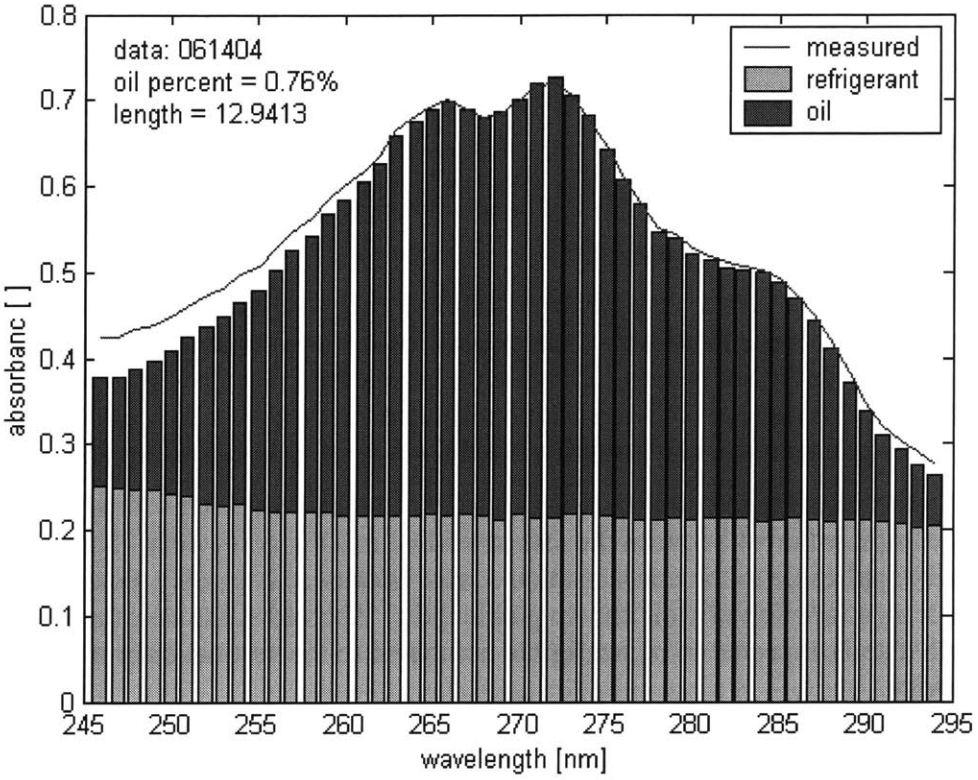

Figure 10: An estimation of the oil (upper bar) and refrigerant (lower bar) contributions to the total absorbance was generated from 0.76% oil concentration data. The red line is the measured data less the baseline absorbance as a check on this estimation.

The importance of the refrigerant's absorption is evident even over the optimal spectrum of wavelengths. Therefore, the absorbance due to the refrigerant cannot be neglected at low oil concentrations. This means that the number of unknown variables during calibration is increased from one to two unknowns for each wavelength used. This is not a problem however, because two or more known samples can be used during calibration to estimate these variables. These calculations will be shown in detail below.

Expanding Equation (5) – now including the refrigerant – gives the following relation for the slope of the absorbance-pathlength line β:

$$\begin{aligned}\beta_{\lambda c} &= \frac{d}{dl}\left(a^{*}_{\lambda cl}\right) \\ &= \varepsilon_{\lambda,oil}c_{oil} + \varepsilon_{\lambda,ref}c_{ref} \\ &= \left(\varepsilon_{\lambda,oil} - \varepsilon_{\lambda,ref}\right)c_{oil} + \varepsilon_{\lambda,ref}\end{aligned} \quad . \tag{16}$$

Methods based on this equation will be referred to as beta methods or linear regression methods that estimate beta. This definition will be the beginning point for the calibration and sensor usage methods that use both components in the mixture.

4.2 Multiple pathlength measurements

Analytical techniques have been discussed for devices that use single and double pathlengths. The differential measurement has the ability to cancel out the baseline absorbance and give a superior estimate of the slope β. However, this estimate can be further improved by using more than two pathlengths. This section will give a technique to use any number of pathlength measurements to improve the estimate. The diminishing advantages of additional pathlengths will also be noted.

In the two pathlength case, the estimation of the slope is the simple solution shown in Equation (13). However, random noise on the absorbance measurement, a^*, will cause errors in the estimation. The differential measurement might even amplify these errors. By using three or more pathlengths, the calculation of the slope changes from an analytical solution to a statistical estimation such as linear regression.

Y-on-x linear regression is a form of linear least squares. This form minimizes the vertical squared error between the estimated line and the noisy data. This method is specifically applicable to the concentration sensor because it has noisy measurements of absorbance as a function of well known pathlengths. Therefore, the horizontal error on pathlength data is expected to be negligible compared to the vertical error on absorbance in this device.

The following equations use a set of pathlengths, $L = [l_1, l_2, \ldots, l_P]$ and the absorbance measurements made at those pathlengths, $A_L = [a_1, a_2, a_P]$. These vectors will be reduced into a scalar – an estimation of the slope, $\beta_{\lambda c}$. As demonstrated in Equation (16), this single parameter is all that will be needed to calibrate and use the sensor. Therefore, all of the pathlength and absorbance data can be reduced into this single value for each wavelength and concentration measured.

The set of equations below are a review of y-on-x linear regression, which is a form of least squares estimation for linear curve fits. The estimation of slope β is given without proof, but a proof can be found in [5].

Average length,

$$\bar{l} = \frac{1}{P}\sum_{p=1}^{P}(l_p) \tag{17}$$

Average absorbance,

$$\bar{a} = \frac{1}{P}\sum_{p=1}^{P}(a_p) \tag{18}$$

Sample variance of pathlength,

$$s_{L,L} = \frac{1}{P}\sum_{p=1}^{P}\left(l_p - \bar{l}\right)^2 . \tag{19}$$

Sample covariance between pathlength and absorbance,

$$s_{L,A_L} = \frac{1}{P}\sum_{p=1}^{P}\left(a_p - \bar{a}\right)\cdot\left(l_p - \bar{l}\right). \tag{20}$$

Estimation of slope,

$$\begin{aligned}\beta &= \rho_{L,A_L}\sqrt{\frac{s_{A_L,A_L}}{s_{L,L}}} \\ &= \frac{s_{L,A_L}}{\sqrt{s_{L,L}\cdot s_{A_L,A_L}}}\sqrt{\frac{s_{A_L,A_L}}{s_{L,L}}} \\ &= \frac{s_{L,A_L}}{s_{L,L}}\end{aligned} . \tag{21}$$

Estimated absorbance line,

$$a - \bar{a} = \beta\left(l - \bar{l}\right). \tag{22}$$

Incidentally, these equations are equivalent to a linear least squares fit, which will be discussed in detail. The plot below uses sample data to show the estimated y-on-x regression line that reduces the vertical distances to the data points.

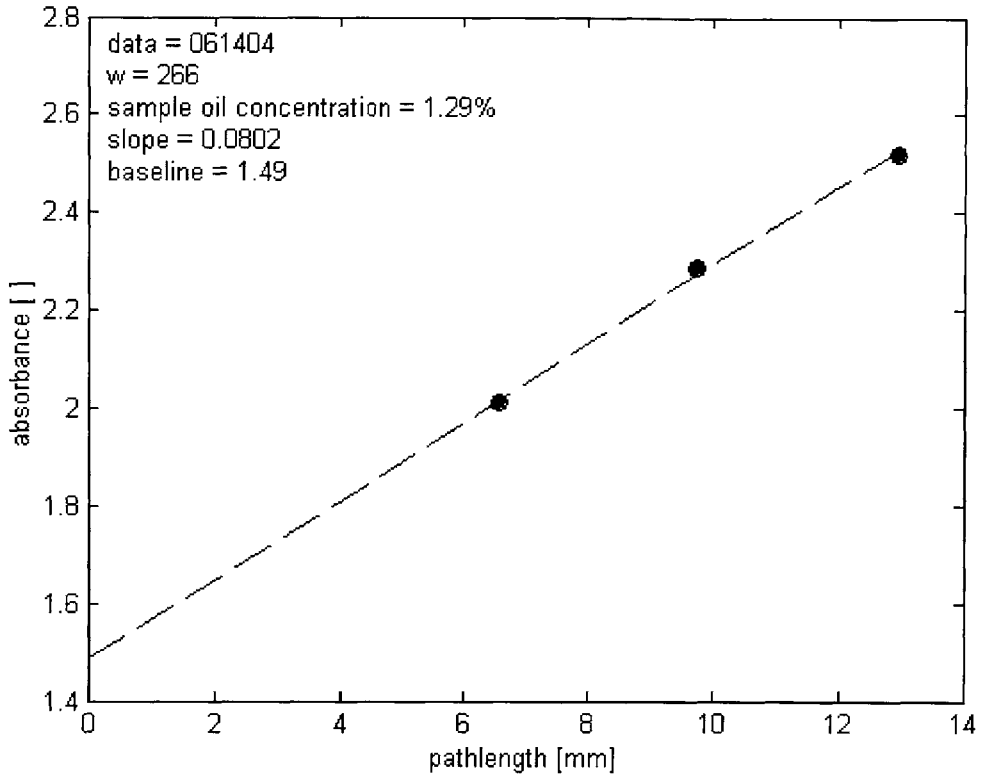

Figure 11: A plot of linear regression on absorbance versus pathlength data. The vertical distance to the data points are minimized in the estimation.

Bounded by probability, the estimation of β approaches the true value as the number of noisy measurements increases. A program was developed to demonstrate the convergence of the linear regression error to zero as the number of pathlengths increases. The model compares a differential technique to a linear regression technique. However, the differential method only uses two pathlengths; so the additional information is unused by it.

In this simulation, noisy data about a known line is used to estimate the true slope of the line, via the equations above. The number of data points is increased as desired, and the estimations and errors are all computed with each increase in the number of points. The plot below shows results from this model – the error from the linear regression estimate is compared to that of the differential estimate in. The simulation shows the expected result: the linear regression squared error has an exponential decay to zero. However, after about three or four pathlengths, the added accuracy of additional pathlengths becomes less significant.

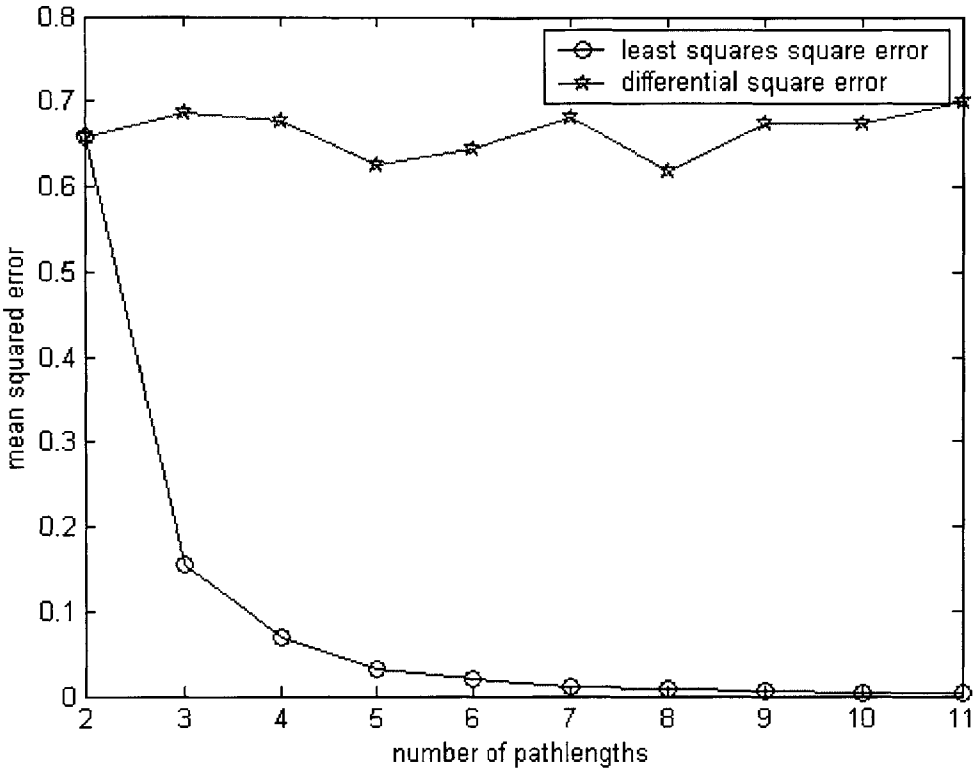

Figure 12: A model showing the least squares reduction in error as number of pathlengths increases. The benefit diminishes after about four or five samples, however.

4.3 Multiple wavelength measurements

Just as with multiple pathlengths, measuring absorbance over multiple wavelengths gives a statistically better oil concentration measurement. However, additional wavelengths are no benefit during calibration – each wavelength requires the calibration of two unknown extinction coefficients (one for the oil and one for the refrigerant). Thus adding new wavelengths means adding new unknown variables to the procedure. However, the new unknowns are no drawback either. They can be estimated from the multitude of data each wavelength produces.

The statistical benefit of the additional wavelengths applies during sensor operation. When the sensor is in use, the data from each wavelength can be manipulated independently to predict the oil concentration in an unknown sample. These redundant predictions can be coordinated by a least squares estimate to reduce the errors caused by noisy measurements.

As discussed above, there should be an optimal wavelength region for each oil and refrigerant combination. It follows that some wavelengths will generate more reliable data that follow the model better than others. Therefore, a metric is needed to select and weight the wavelengths that will be used to estimate concentration. A performance metric will be presented below to rank the reliability of each wavelength.

4.3.1 Wavelength performance metric

A metric can be created that ranks how well the data agrees with the Beer-Lambert model: the better the data matches the model, the better performance that wavelength will contribute to the sensor's predictions. The main behavior sought in the absorbance data is linearity with both pathlength and concentration. According to the model, the absorbance is completely linear with oil concentration and optical pathlength:

$$\begin{aligned} a_{\lambda cl} &= \left(\varepsilon_{\lambda,oil} c_{oil} + \varepsilon_{\lambda,ref} c_{ref}\right) l \\ &= \left(\varepsilon_{\lambda,oil} c_{oil} + \varepsilon_{\lambda,ref} \left[1 - c_{oil}\right]\right) l \\ &= \left(\left[\varepsilon_{\lambda,oil} - \varepsilon_{\lambda,ref}\right] c_{oil} + \varepsilon_{\lambda,ref}\right) l \end{aligned} . \tag{23}$$

Therefore, the performance metric for a wavelength can be a measure of how linear it tends to be with these two variables. The sum of squared error (SSE) between the data points and the fitted line is used as the basis for quantitatively ascribing goodness of a fit. But the SSE needs to be normalized so that high absorbance measurements are not penalized. To the contrary, wavelengths with a high absorbance measurement are more valuable. These wavelengths have a higher oil extinction coefficient; thus they make the device more sensitive to oil. The R^2 value, or coefficient of determination can be defined as:

$$\begin{aligned} R^2 &= 1 - \alpha\left[\frac{SSE}{SST}\right] \\ &= 1 - \alpha\left[\frac{\sum_{n=1}^{N}\left(Y_n - \hat{Y}_n\right)^2}{\sum_{n=1}^{N}\left(Y_n^2\right) - \frac{\left(\sum_{n=1}^{N}\left(Y_n\right)\right)^2}{N}}\right], \end{aligned} \tag{24}$$

where the data set Y is the noisy data and the set $\hat{Y}$ is the fitted line. Alpha is a parameter used to make the weighting more or less severe. A value of 10 was used for the weighting shown below.

A perfect fit has zero squared error, thus $R^2 = 1$. A poor fit will have an R^2 value near 0. The plot below shows absorbance data from calibration samples plotted against concentration for three pathlengths.

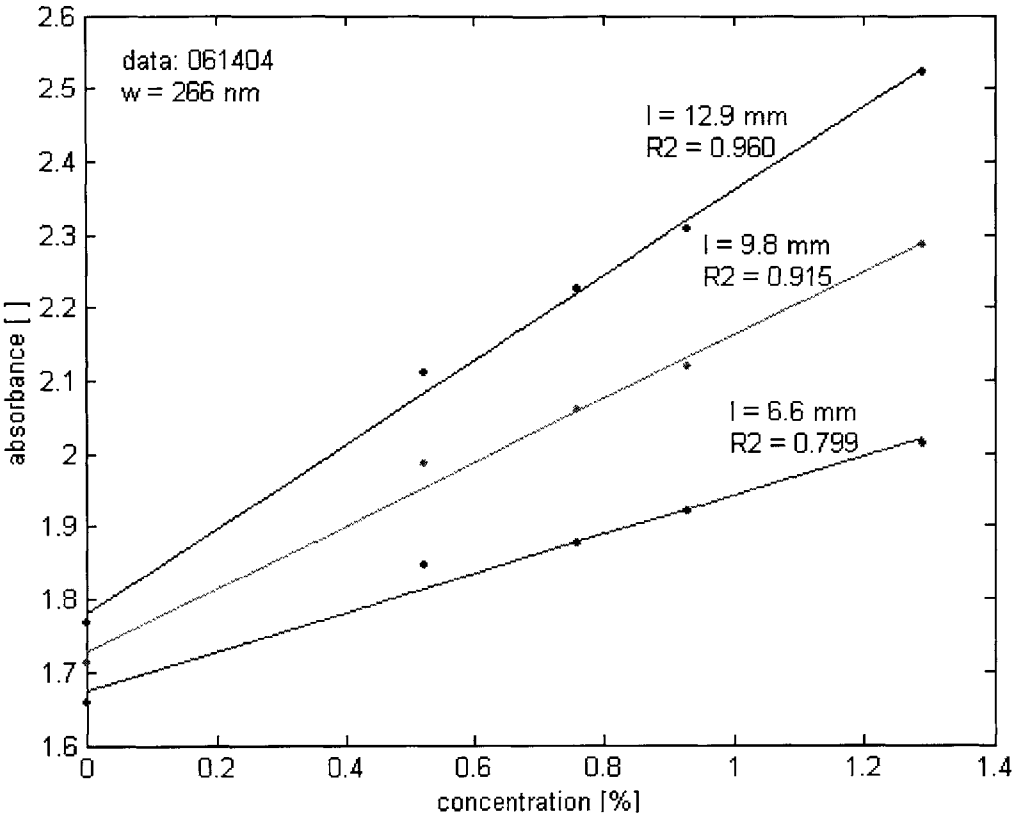

Figure 13: A plot of concentration linearity as a performance metric for wavelengths. This plot also shows a trend in the pathlengths that suggests longer pathlengths give more reliable readings.

The coefficient of determination, R^2, can be calculated for each line at each wavelength. A symmetric process can be performed for absorbance linearity with pathlength. This calculation will use the same data but create a line for each sample concentration. These procedures give an abundance of data to determine a weighting value for each wavelength.

The plot below shows the R^2 values calculated for all wavelengths. There is clearly an optimal point across wavelengths that will have the best agreement with the model. This point happens to coincide with the wavelength of the left peak in the oil extinction data seen in Figure 6.

Most of the zero values in the plot below were set in a logical decision because they violated a rule. For example, if at a particular wavelength had data where an oil concentration of 1% had a lower absorbance than that of an oil concentration of 0.5%, then this wavelength was deemed unreliable. This occurs very often on the left and right sides of the two peaks near 270 nm (see Figure 6).

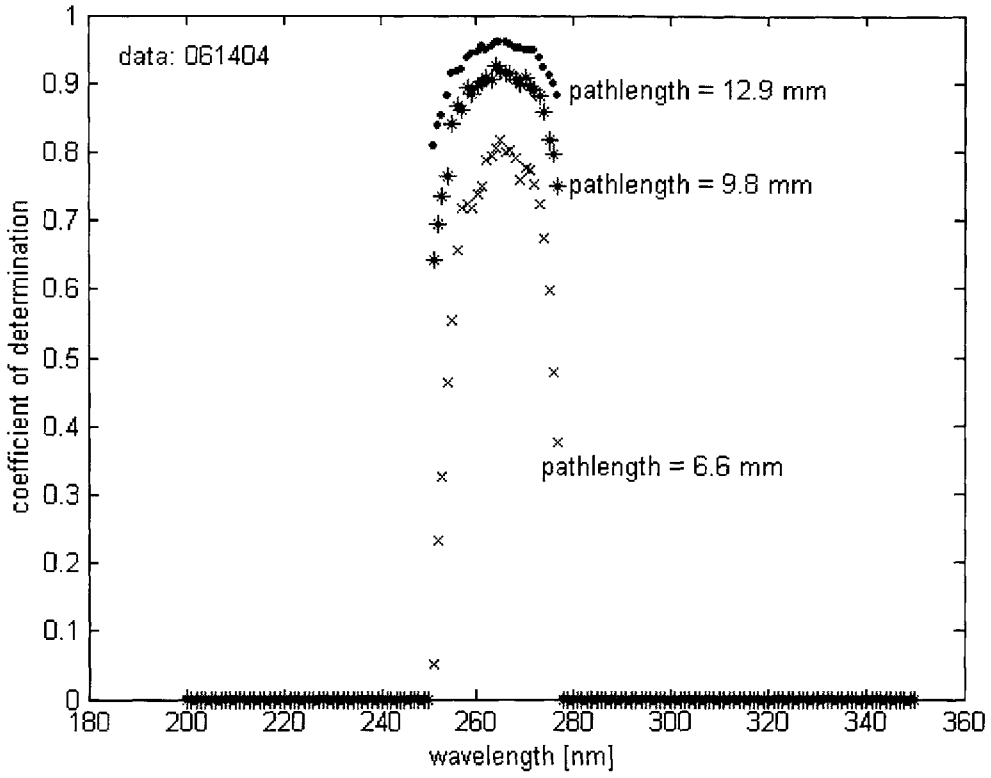

Figure 14: A plot of the coefficient of determination for concentration linearity shows an optimal point for making oil concentration estimates. The wavelengths with higher coefficient values should follow the model more accurately.

This metric can be used to generate a weighting vector that will be used in the weighted least squares method shown later.

5 Calibration technique

Calibrating the sensor is the process of estimating the unknown extinction coefficients of the oil and refrigerant. The refrigerant absorbance can be measured as a pure fluid, whereas the oil absorbs too much light intensity to be measured at high concentrations. The analysis of a mixture where only one substrate accounts for the absorbance was shown in Equation (8). The analysis is the same for a pure substance but will be repeated here briefly for the refrigerant. Procedures for calibrating the oil as a two part mixture will then be given.

5.1 Calibrating the pure refrigerant

The measured absorbance in the pure refrigerant can be broken down into two parts: the baseline absorbance and the absorbance due to the refrigerant. This is expressed as

$$a^*_{\lambda l} = a_{baseline+}\varepsilon_{\lambda,ref}c_{ref}l$$
$$= a_{baseline+}\varepsilon_{\lambda,ref}l \quad . \tag{25}$$

Note that for a pure substance the concentration, c, is identically 1; thus it can be disregarded below. The linear regression of absorbance on pathlength will consolidate the absorbance data for each pathlength into the estimated slope, β_λ. For the pure refrigerant the slope is equal to the extinction coefficient. Note the similarity of the equation below to Equation (13)

$$\beta_{\lambda,ref} = \varepsilon_{\lambda,ref} \, . \tag{26}$$

This is an intuitive result, considering that the definition of the extinction coefficient is absorbance per unit length – the same meaning as the slope of absorbance versus pathlength.

5.2 Calibrating the oil

5.2.1 Calibrating the pure oil

As explained above, determining the extinction coefficients of a pure substance is straightforward. But given its high extinction coefficient, this is unpractical for the oil. Consider the pathlength necessary to measure pure oil. The peak absorbance rate of the oil FVC50k is around 5.5 [1/mm]. The minimum readable light transmission of the spectrophotometer (a Cary50 model by Varian Inc.) is near 0.1%. This transmission corresponds to an absorbance of 3, shown below.

$$T = 0.1\% = 0.001 = 10^{-3}$$
$$a = \log\left(\frac{1}{T}\right) = \log\left(10^3\right) = 3 \, . \tag{27}$$

Thus, accounting for baseline absorbance, the maximum readable pathlength is shown to be

$$l_{\max} = \frac{a^*_{\max} - a_{baseline}}{\varepsilon_{\max}} = \frac{3 - 1.4}{5.5\left[\frac{1}{mm}\right]} = 0.29[mm]. \tag{28}$$

This means the sample would have to be put in a chamber less than half a millimeter wide. Calibrating oil with a pure sample presents three problems. First, the calibration should be performed near the intended concentration range – 0 to 1 percent oil concentration. Second, the readable pathlength is so small that any wall effects, impurities, and non-uniformities in the sample may create large errors in the reading. Third, fabricating the channel geometry at this scale is difficult to do in a cost effective

way while still maintaining the necessary tolerances for calibration. For these reasons, the oil is calibrated as a two part mixture.

5.2.2 Calibrating a two part mixture

Although the extinction coefficients of the refrigerant may be solved separately, the analysis below assumes that all the extinction coefficients are unknown. The starting point of this analysis is an intermediate line from Equation (16) and is repeated here for convenience:

$$\beta_{c,\lambda} = \varepsilon_{oil,\lambda} c_{oil} + \varepsilon_{ref,\lambda} c_{ref} \,. \tag{29}$$

$\beta_{\lambda c}$ is reduced via linear regression of the absorbance and pathlength data, and the concentrations, c_{oil} and c_{ref}, are known. Therefore, with two calibration samples, the two unknowns, $e_{\lambda,oil}$ and $e_{\lambda,ref}$, can be solved algebraically. However, N>2 calibration samples will give a statistically better estimate of the extinction coefficients and train the data over the entire operating range. The N samples will yield the following N equations:

$$\begin{aligned}
\beta_{1,\lambda} &= \varepsilon_{oil,\lambda} c_{1,oil} + \varepsilon_{ref,\lambda} c_{1,ref} \\
\beta_{2,\lambda} &= \varepsilon_{oil,\lambda} c_{2,oil} + \varepsilon_{ref,\lambda} c_{2,ref} \\
&\text{M} \\
\beta_{N,\lambda} &= \varepsilon_{oil,\lambda} c_{N,oil} + \varepsilon_{ref,\lambda} c_{N,ref}
\end{aligned} \,. \tag{30}$$

This is a typical least squares problem. Noisy measurements of absorbance, a*, yield erroneous estimations of $\beta_{n,\lambda}$. The redundant measurements will help to reduce these errors. A general treatment of this problem can be found in [6]. The equation above can be written in matrix form as

$$\beta_{n,\lambda} = c_n^T e_\lambda \,, \tag{31}$$

where

$$c_n^T = \begin{bmatrix} c_{n,oil} & c_{n,ref} \end{bmatrix} \in R^{1x2} \text{, and} \tag{32}$$

$$e_\lambda = \begin{bmatrix} \varepsilon_{oil,\lambda} \\ \varepsilon_{ref,\lambda} \end{bmatrix} \in R^{2x1} \,. \tag{33}$$

The objective is to minimize J, the sum of the squared error, by choosing the optimal values for e_λ:

$$J = \sum_{n=1}^{N} \left(c_n^T \hat{e}_\lambda - \beta_{n,\lambda} \right)^2 . \tag{34}$$

The optimal values can be found by setting the derivative of the summation to zero:

$$\begin{aligned} \nabla_{\hat{e}_\lambda} J &= 2 \sum_{n=1}^{N} c_n \left(c_n^T \hat{e}_\lambda - \beta_{n,\lambda} \right) \\ &= 0 \end{aligned} . \tag{35}$$

Thus, rearranging the equation above gives

$$\sum_{n=1}^{N} c_n c_n^T \hat{e}_\lambda = \sum_{n=1}^{N} c_n \beta_{n,\lambda} . \tag{36}$$

And the e_λ matrix can be moved out of the summation because it does not depend on n.

$$\left(\sum_{n=1}^{N} c_n c_n^T \right) \cdot \hat{e}_\lambda = \sum_{n=1}^{N} c_n \beta_{n,\lambda} \tag{37}$$

Finally, a left sided multiplication of the inverse of the concentration matrix solves for the estimation of extinction coefficients, e_λ shown below.

$$\begin{bmatrix} \hat{\varepsilon}_{oil,\lambda} \\ \hat{\varepsilon}_{ref,\lambda} \end{bmatrix} = \hat{e}_\lambda = \left(\sum_{n=1}^{N} c_n c_n^T \right)^{-1} \sum_{n=1}^{N} c_n \beta_{n,\lambda} . \tag{38}$$

The solution can be written more succinctly by defining two more matrices.

$$C = \begin{bmatrix} c_1^T \\ c_2^T \\ \mathrm{M} \\ c_N^T \end{bmatrix} = \begin{bmatrix} c_{1,oil} & c_{1,ref} \\ c_{2,oil} & c_{2,ref} \\ \mathrm{M} & \mathrm{M} \\ c_{N,oil} & c_{N,ref} \end{bmatrix} \in R^{Nx2} \text{, and} \tag{39}$$

$$b_\lambda = \begin{bmatrix} \beta_{1,\lambda} \\ \beta_{2,\lambda} \\ \mathrm{M} \\ \beta_{N,\lambda} \end{bmatrix} \in R^{Nx1} . \tag{40}$$

It is easy to show that

$$\sum_{n=1}^{N} c_n c_n^T = \begin{bmatrix} c_1 & c_2 & \Lambda & c_N \end{bmatrix} \begin{bmatrix} c_1^T \\ c_2^T \\ \mathrm{M} \\ c_N^T \end{bmatrix} = \left(C^T C\right), \tag{41}$$

and

$$\sum_{n=1}^{N} c_n \beta_{n,\lambda} = \begin{bmatrix} c_1 & c_2 & \Lambda & c_N \end{bmatrix} \begin{bmatrix} \beta_{1,\lambda} \\ \beta_{2,\lambda} \\ \mathrm{M} \\ \beta_{N,\lambda} \end{bmatrix} = C^T b_\lambda . \tag{42}$$

Using these substitutions, Equation (37) becomes

$$\left(C^T C\right) \cdot \hat{e}_\lambda = C^T b_\lambda , \tag{43}$$

and e_λ can be solved for by inverting the matrix on the left side again:

$$\begin{bmatrix} \hat{\varepsilon}_{oil,\lambda} \\ \hat{\varepsilon}_{ref,\lambda} \end{bmatrix} = \hat{e}_\lambda = \left(C^T C\right)^{-1} C^T b_\lambda . \tag{44}$$

The benefit of this matrix representation is that all the wavelength data can be brought into a single expression without changing the form of the equation above. The two matrices that depend on wavelength, e_λ and B_λ, can be expanded from a vector to a two dimensional matrix to account for the full set of wavelength data. The higher dimension definitions are shown below:

$$E = \begin{bmatrix} e_1 & e_2 & \Lambda & e_M \end{bmatrix} = \begin{bmatrix} \varepsilon_{oil,1} & \varepsilon_{oil,2} & \Lambda & \varepsilon_{oil,M} \\ \varepsilon_{ref,1} & \varepsilon_{ref,2} & & \varepsilon_{ref,M} \end{bmatrix} \in R^{2xM} \tag{45}$$

$$B = \begin{bmatrix} b_1 & b_2 & \Lambda & b_M \end{bmatrix} = \begin{bmatrix} \beta_{1,1} & \beta_{1,2} & \Lambda & \beta_{1,M} \\ \beta_{2,1} & \beta_{2,2} & \Lambda & \beta_{2,M} \\ \mathrm{M} & \mathrm{M} & \mathrm{O} & \mathrm{M} \\ \beta_{N,1} & \beta_{N,2} & \Lambda & \beta_{N,M} \end{bmatrix} \in R^{NxM} \tag{46}$$

Finally, the 2xM array of unknown extinction coefficients can be estimated in one succinct line. The expanded form of Equation (43) is

$$\left(C^T C\right)\cdot \hat{E} = C^T B, \tag{47}$$

which leads to the familiar solution

$$\hat{E} = \left(C^T C\right)^{-1} C^T B. \tag{48}$$

This solution gives exactly the same result as applying Equation (44) for each wavelength. Note that the matrix of concentrations, C, is determined by the calibration test operator. The inverse can be guaranteed on that account. Furthermore, the constraint $c_{ref} = 1\text{-}c_{oil}$ ensures that none of the c_n matrices will be scaled versions of each other; therefore, the C matrix will always be full rank and invertible.

Notice that this technique gives extinction coefficients for the refrigerant as well as the oil. These results can be compared to the estimations made from the pure refrigerant, as described in the previous section. If the data fits the linear model well, then these two estimations of the refrigerant properties will agree. The plot below shows the accurate agreement of these two methods made from five sample concentrations between 0 and 1.2% oil concentration.

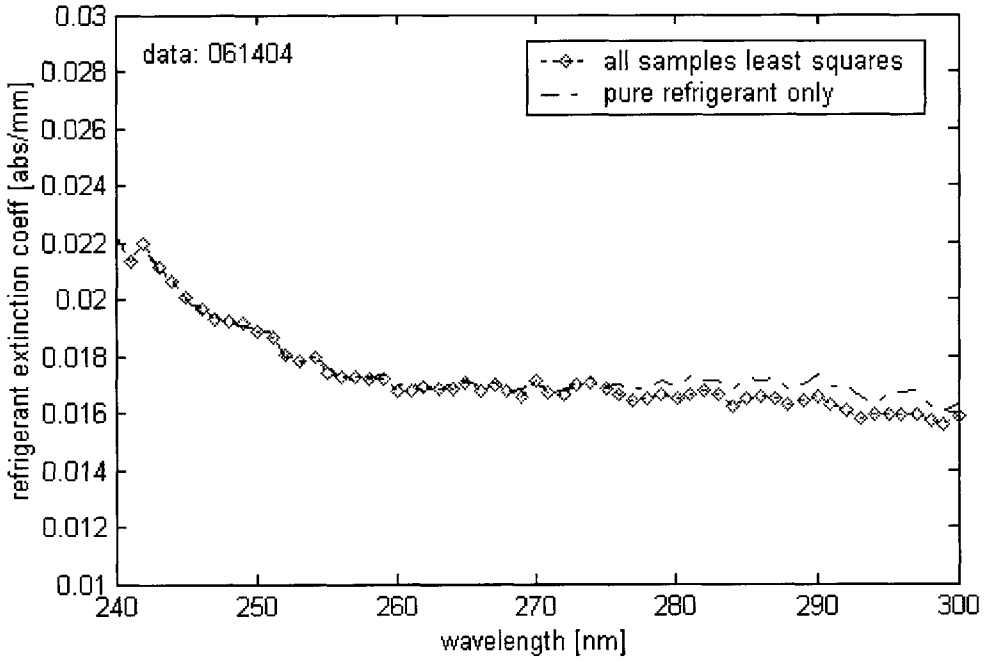

Figure 15: A pure substance calibration and a least squares calibration of multiple samples agree with good accuracy.

5.3 Calibration conditions and assumptions

Calibration is ideally performed at the conditions of the intended use of the sensor. The extinction coefficients of the substrates have a complex dependency on interrelated properties such as temperature, pressure, and density. Furthermore, the online experiment measures the dynamic OCR, not the static oil concentration. Thus, the calibration should use a flowing sample at a controlled temperature, pressure and flow rate.

However, the only way to truly simulate the conditions of the HVAC and control the OCR at the same time is to use an oil free compressor and control the injection rate of the test lubricant. Because these devices were not available, a substitute fluid, isopropyl alcohol, was used to replace the refrigerant and dilute the oil for calibration. This calibration procedure was repeated with a second substitute fluid, R141b, to check that the calibrated values were in agreement. The plot below shows the agreement between the two calibrations and validates the procedure of switching the base refrigerant. The oil extinction coefficients are within 5 to 10% agreement. The isopropyl data is more trusted because it is from a less volatile fluid. In fact refrigerant R141b's strong tendency to evaporate may explain the error between the two estimates. During calibration with R141b, the oil concentration can become higher than measured, thus causing the estimation of the oil extinction coefficient to be erroneously high.

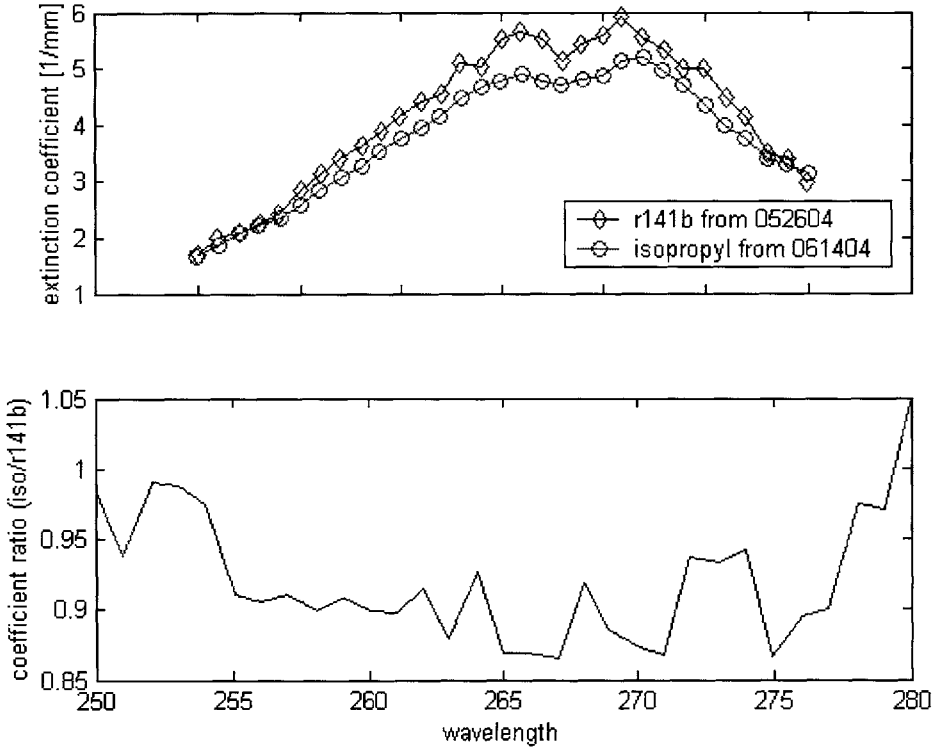

Figure 16: The agreement of two oil calibrations validate the assumption that calibration from a convenient fluid can be used to measure the real refrigerant. The lower plot shows the ratio of the data sets, which are in approximately 95% agreement.

6 Sensor usage after calibration

Once the extinction coefficients of the oil and the refrigerant have been estimated, the sensor is calibrated and ready for use. Two techniques will be presented here: least squares and least squares with weighting. Again, general treatment of this kind is available in [6].

6.1 Least squares estimation of the oil concentration

Applying linear least squares to estimate the oil concentration is very similar to estimating the extinction coefficients. Just as with the calibration analysis, the result from Equation (29) is repeated as the foundation for the sensor usage analysis:

$$\beta_{c,\lambda} = \varepsilon_{oil,\lambda} c_{oil} + \varepsilon_{ref,\lambda} c_{ref} .$$

At first glance, the problem seems indifferent to which set of variables (the extinction coefficients or the concentrations) is known and which is not. But the constraint from Equation (6) reduces the number of unknown concentrations to one. Applying the constraint yields the result given in Equation (16):

$$\beta_{\lambda c} = \left(\varepsilon_{\lambda,oil} - \varepsilon_{\lambda,ref}\right) c_{oil} + \varepsilon_{\lambda,ref} .$$

Because coil is the only unknown, the algebraic solution can be found from just one wavelength:

$$\hat{c}_{\lambda,oil} = \frac{\beta_{\lambda c} - \varepsilon_{\lambda,ref}}{\varepsilon_{\lambda,oil} - \varepsilon_{\lambda,ref}} . \tag{49}$$

But as stated before, multiple wavelengths will be used to reduce noise in the measurements and provide a statistically better estimate. The equation above can be rearranged to the form that is typical of a least squares problem with M wavelengths:

$$\begin{aligned} \left(\beta_1 - \varepsilon_{1,ref}\right) &= \left(\varepsilon_{1,oil} - \varepsilon_{1,ref}\right) c_{oil} \\ \left(\beta_2 - \varepsilon_{2,ref}\right) &= \left(\varepsilon_{2,oil} - \varepsilon_{2,ref}\right) c_{oil} \\ &\text{M} \\ \left(\beta_M - \varepsilon_{M,ref}\right) &= \left(\varepsilon_{M,oil} - \varepsilon_{M,ref}\right) c_{oil} \end{aligned} . \tag{50}$$

The objective is to minimize the sum of squared errors by finding the optimal oil concentration. This function is

$$J = \sum_{m=1}^{M} \left(\left(\varepsilon_{m,oil} - \varepsilon_{m,ref}\right) \hat{c}_{oil} - \left(\beta_m - \varepsilon_{m,ref}\right) \right)^2 . \tag{51}$$

Setting the derivative of the expression to zero to find the minimum gives:

$$\frac{dJ}{d\hat{c}_{oil}} = 2\sum_{m=1}^{M}\left(\varepsilon_{m,oil}-\varepsilon_{m,ref}\right)\left(\left(\varepsilon_{m,oil}-\varepsilon_{m,ref}\right)\hat{c}_{oil}-\left(\beta_m-\varepsilon_{m,ref}\right)\right) \\ =0 \qquad (52)$$

Solving for the optimal estimate yields:

$$\hat{c}_{oil} = \frac{\sum_{m=1}^{M}\left(\varepsilon_{m,oil}-\varepsilon_{m,ref}\right)\left(\beta_m-\varepsilon_{m,ref}\right)}{\sum_{m=1}^{M}\left(\varepsilon_{m,oil}-\varepsilon_{m,ref}\right)\left(\varepsilon_{m,oil}-\varepsilon_{m,ref}\right)}. \qquad (53)$$

Although the numerator and denominator are scalars, Equation (53) can be written in a matrix form using the following set of definitions:

$$\Delta\varepsilon_m = \varepsilon_{m,oil}-\varepsilon_{m,ref}$$
$$\Delta\mathrm{E}^T = \left[\Delta\varepsilon_1 \quad \Delta\varepsilon_2 \quad \Lambda \quad \Delta\varepsilon_M\right] \in R^{1xM}$$
$$\Delta\beta_m = \beta_m-\varepsilon_{m,ref} \qquad (54)$$
$$\Delta\mathrm{B} = \left[\Delta\beta_1 \quad \Delta\beta_2 \quad \Lambda \quad \Delta\beta_M\right]^T \in R^{Mx1}$$

Equation (53) can then be written succinctly as

$$\hat{c}_{oil} = \frac{\Delta E^T \Delta B}{\Delta E^T \Delta E}. \qquad (55)$$

This form of the solution will prove useful when dealing with weighted measurements in the next section.

6.2 Weighted least squares estimation

Each wavelength used in the calibration is capable of estimating the oil concentration. But some wavelengths have been shown to be more reliable than others. Indeed, at some wavelengths where the extinction coefficient is changing rapidly the measurements show much more randomness than others. The performance metric discussed previously shows an organized valuation of the wavelengths. Such a result is certainly not due to random chance. The plot below shows the final vector used to weight the wavelengths. These values are the product of all the R^2 values from the linearity with pathlength and concentration calculations.

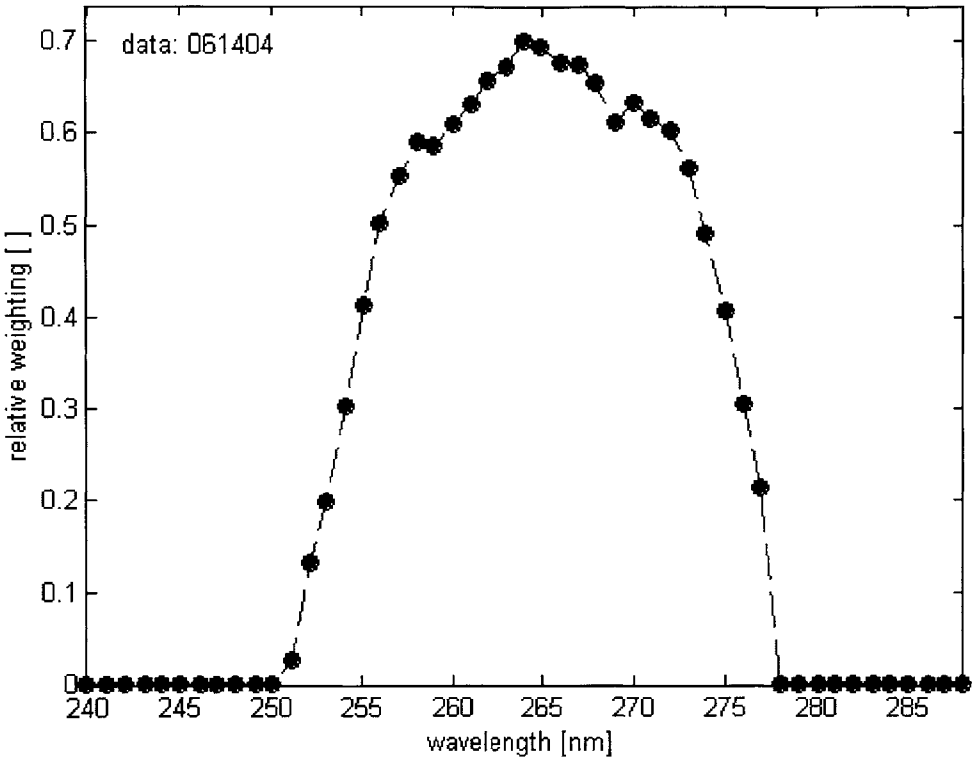

Figure 17: The wavelength weighting vector created from the measured absorbance's linearity with pathlength and concentration. The optimal point at 263 nanometers was used for techniques that only avail one wavelength measurement.

This metric can be used to assign a weighting to each wavelength, thus controlling the relative effect of each measurement. A relative value is assigned to each wavelength, creating a vector of weightings: $[w_1, w_2, \ldots, w_M]$. Thus a diagonal matrix of weightings can be defined as:

$$W = \begin{bmatrix} w_1 & 0 & \Lambda & 0 \\ 0 & w_2 & & \\ \mathrm{M} & & \mathrm{O} & \\ 0 & & & w_M \end{bmatrix} \in R^{MxM} . \tag{56}$$

The objective function to minimize can be defined as a weighted sum:

$$J = \sum_{m=1}^{M} \left(\left(\varepsilon_{m,oil} - \varepsilon_{m,ref} \right) \hat{c}_{oil} - \left(\beta_m - \varepsilon_{m,ref} \right) \right)^2 w_m . \tag{57}$$

And the analysis follows as before:

$$\frac{dJ}{d\hat{c}_{oil}} = 2\sum_{m=1}^{M}\left(\varepsilon_{m,oil}-\varepsilon_{m,ref}\right)w_m\left(\left(\varepsilon_{m,oil}-\varepsilon_{m,ref}\right)\hat{c}_{oil}-\left(\beta_m-\varepsilon_{m,ref}\right)\right) = 0 \quad (58)$$

Solving the above equation for the oil concentration estimate yields:

$$\hat{c}_{oil} = \frac{\sum_{m=1}^{M}\left(\varepsilon_{m,oil}-\varepsilon_{m,ref}\right)w_m\left(\beta_m-\varepsilon_{m,ref}\right)}{\sum_{m=1}^{M}\left(\varepsilon_{m,oil}-\varepsilon_{m,ref}\right)w_m\left(\varepsilon_{m,oil}-\varepsilon_{m,ref}\right)}, \quad (59)$$

which can be written in matrix form as

$$\hat{c}_{oil} = \frac{\Delta E^T W \Delta B}{\Delta E^T W \Delta E}. \quad (60)$$

7 Implementation

7.1 Overview of the spectrophotometer and optical network

The Cary50, by Varian Inc., was the spectrophotometer in these experiments. The instrument controls the wavelength of light and measures the incident and transmitted light intensities. This unit has a fiber optic probe accessory which allows the incident light to freely travel to a remote test setup. This extension is necessary to optically connect the instrument to the pressure vessel that gives light access to a sample of fluid within the high pressure HVAC system. The image below shows the spectrophotometer, its dedicated computer for data acquisition, and the fiber optic probes extending to a remote calibration stand.

The fiber optic cables give needed versatility, but this has a drawback as well: the system's baseline absorbance suddenly change when the wires move. The fiber optic cables transmit the light via total internal reflection. If a bend or kink in the cable exceeds a critical angle, then the light will not have total reflection, rather some will transmit through the cable. This means that the cables must be carefully arranged to make consistent measurements.

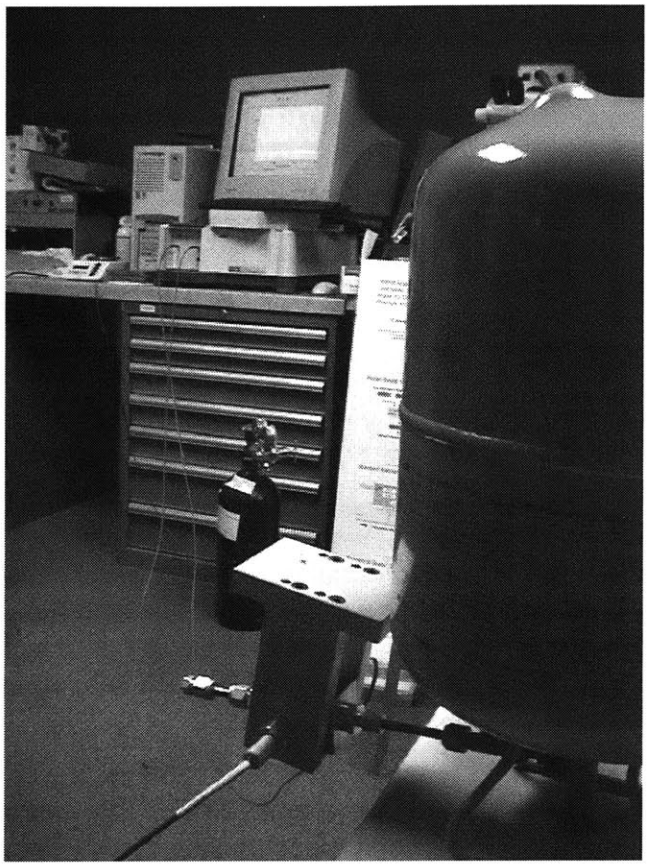

Figure 18: Image of the fiber optic cables and probes that give the spectrophotometer the versatility to make measurements on difficult to access samples.

7.2 Sensor design

Two oil concentration sensor vessels were designed to be installed and operated with an industrial air conditioner. The first design is a single pathlength device that was used to test the concept. The second design is a three-pathlength device that has provided all of the absorbance data in this report. For both designs duplicate units were constructed so that calibration was performed with a test unit while the dedicated unit was connected to the air conditioner. The vessel was designed to meet the following objectives:

1. provide optical path(s) through the working fluid
2. prevent the formation of bubbles
3. seal the high pressure, flowing fluid

The image below is from the first design, and it shows most of the major design concepts: quartz windows, rubber gaskets, and a three part brass body assembly.

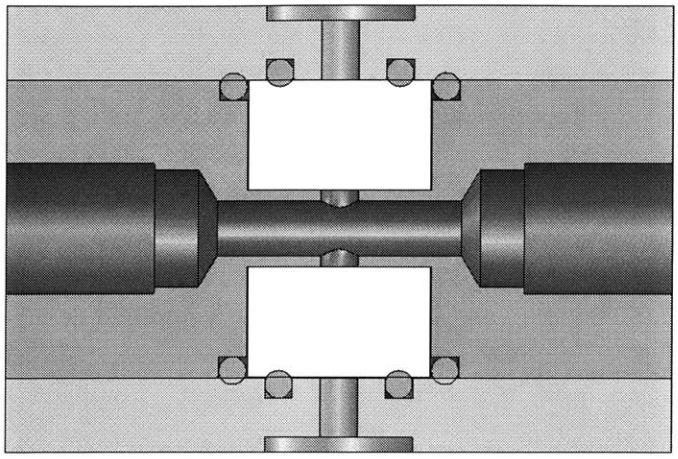

Figure 19: solid model cross-section of original vessel design

Silica fused quartz windows were used to provide the optical path through the pressurized fluid. This polished quartz is one of the few materials that can transmit nearly 95% of the light intensity at these wavelengths. The material is difficult to machine because it is a brittle glass; cracking and chipping is a concern for these parts. The quartz windows were made conservatively thick (3/8") to resist any warping of the flat surfaces and to prevent rupturing under pressure.

Rubber gaskets were used to seal the two leak paths around the quartz. They were designed extremely tightly such that they compress 25% of their volume when the assembly is screwed together. The compressible gaskets have the added benefit of taking up any slack on the quartz pieces. This allows the low-tolerance quartz parts to be undersized by about ten thousandths of an inch to ensure a slip fit into the pocket. The large gasket seals around the outer perimeter of the quartz cylinder, preventing leaks from propagating through the interface of the mating brass plates. The small gasket seals between the quartz and the brass plate, preventing leaks from propagating through the optical viewing ports (shown as vertical pathways in the image above). An image of the first vessel design is below:

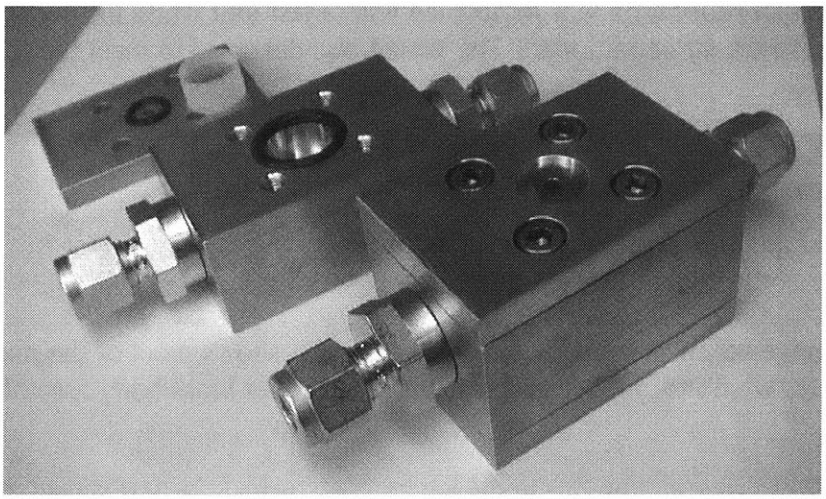

Figure 20: image of the original vessel design

The image above shows a circular pocket in the center of the screws. This is a locating feature for the fiber optic probe tips. Alignment of the probe tips is critical to lowering the total absorbance of the device, thus increasing the readable oil concentration range.

The second vessel design uses the same pocket geometry as the first vessel. This was done so that identical quartz and gasket parts could be used in each pathway. This design was made longer and wider to provide three optical pathlengths. The image below shows the final multiple pathlength design:

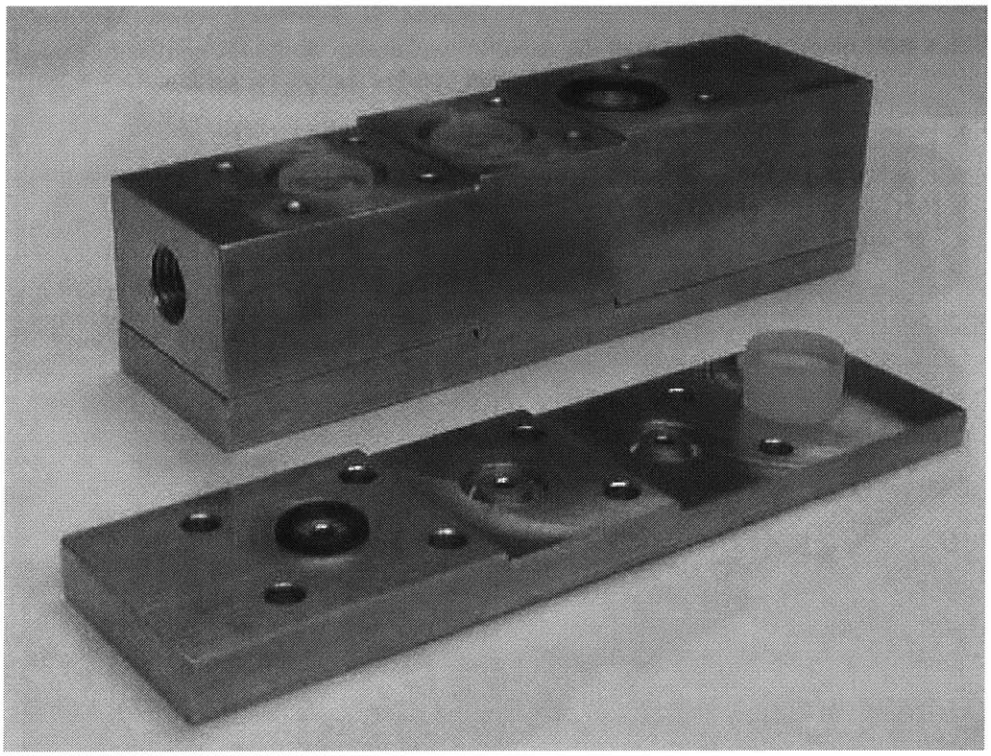

Figure 21: An image of the second vessel design and replaceable parts.

The flow is turbulent in the device, with the Reynolds number varying from 20,000 to 50,000 at the large hole and the small hole, respectively. As a result of the high Reynold's number bubble formation was a concern in the design. The contracting flow passage in the device prevents bubbles from developing through the changing diameter. As the flow area decreases, the velocity of the fluid increases, and the fluid experiences a Bernoulli pressure drop. This favorable pressure gradient is stable; thus no eddy currents should form nor should the flow separate. The following two images are cross-sectional views that show the three pathlengths through the device.

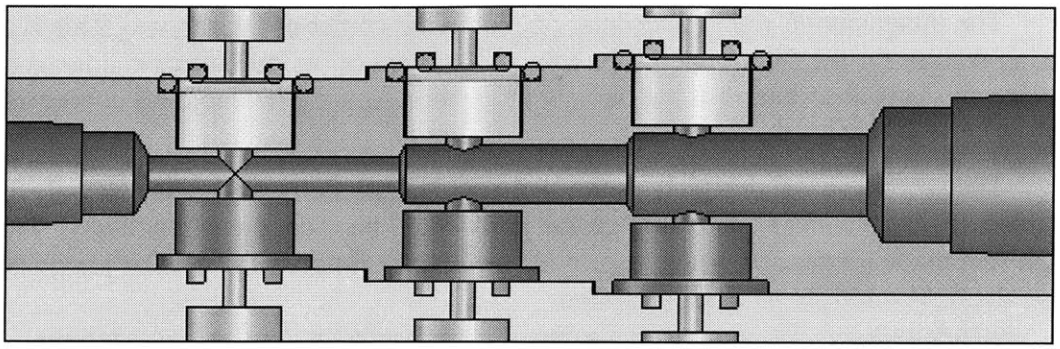

Figure 22: A solid model cross-section of the second vessel design shows the contracting passages that vary the optical pathlengths and prevent bubble formation.

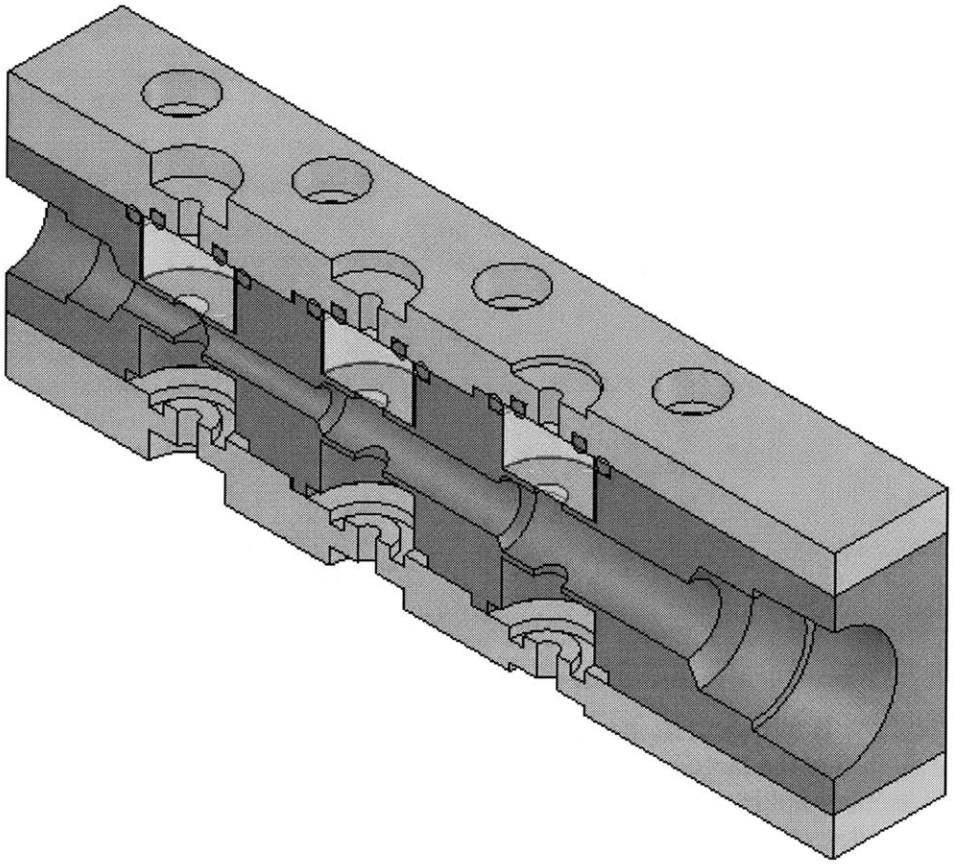

Figure 23: An isometric sectional view of second vessel design.

The vertical pathways in the image above are the optical paths between the probe tips. Each pathway was designed such that from incident-tip to transmitted-tip, every aspect is identical except one: the fluid pathlength. The length of open air, the length of fused silica quartz, and the length of the dead volume are the same in each pathway. This symmetry is crucial so that in a differential or linear regression estimate of the slope β, all of the losses associated during that length of the pathway cancel out as if they were a part of the baseline absorbance. To create this effect, the brass parts had to have three steps, mirroring the step size in the fluid pathlength. The steps in the brass parts are emphasized in the separation of the parts in the image below:

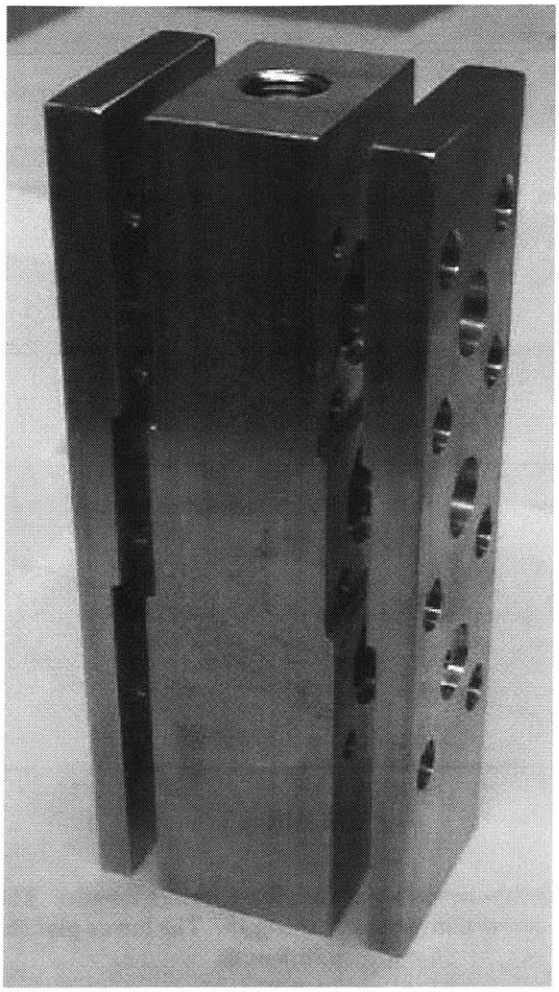

Figure 24: The step design of the second vessel creates multiple optical paths with identical geometry and materials except for the pathlength through the fluid sample.

The most critical features of the design are the lengths of the three paths through the working fluid. A simple model was prepared that used the maximum observed oil extinction coefficient to determine the maximum pathlength and concentration pair that the spectrophotometer could read. From initial inline experiments with the first vessel design, the desired operating range was determined to be 0 to 1 percent oil (by volume). The Cary50 has an upper limit on absorbance of 3.3. But to be conservative, the longest pathlength was designed to give an absorbance of 2.5. And with estimates of the extinction coefficients, the maximum pathlength can be directly calculated from these inputs. The results from this design model are shown in the plot below.

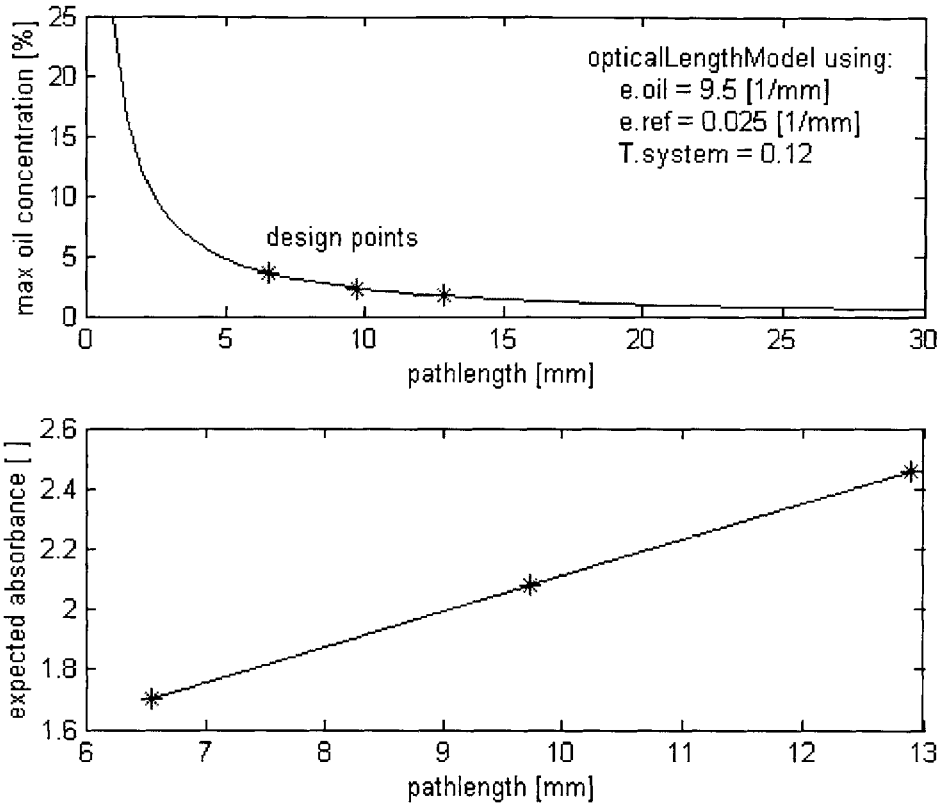

Figure 25: An optical design model shows the three design lengths. The upper plot shows the maximum readable oil concentration versus pathlength. The lower plot shows the absorbance versus pathlength.

This sensor was specifically designed to measure low oil concentrations, thus relativelylow absorbance values. Therefore the pathlength could extend much longer than it would have if the operating range needed to measure up to 5 or 10 percent oil concentration.

One backwards aspect of working with absorbance is the concept of the measured signal. The spectrophotometer is truly measuring the light intensities, which are converted to a transmission as a percentage. The higher the measured transmission is, the lower the absorbance is, and vice versa. Thus when a high absorbance is measured, the signal is actually extremely small. At small signals, the noise of the device becomes a concern as it has a larger corruptive effect on the measurements. Therefore, this device is limited by a high absorbance value, which correlates to a small transmission signal dropping below the resolution of the device towards zero.

But as with all sensors, a trade-off exists between measuring a large operating range of oil concentrations and having a high resolution within those measurements. The resolution of this oil concentration sensor depends not only on the operating range of its use but on the accuracy of the spectrophotometer and the accuracy of the calibration as well. Indication of the device's accuracy is presented in the results.

7.3 Application to the product

As stated above, the sensor was designed to be installed in an industrial air conditioner. Swagelok compression fittings connect copper tubing to the sensor body through NPT adapters. The vessel design places the sensor at the outlet of the condenser, where the fluid is most likely to be liquid rather than a gaseous or two-phase mixture as is prevalent in much of the system. The generic HVAC cycle below has the addition of an oil sensor installed as described.

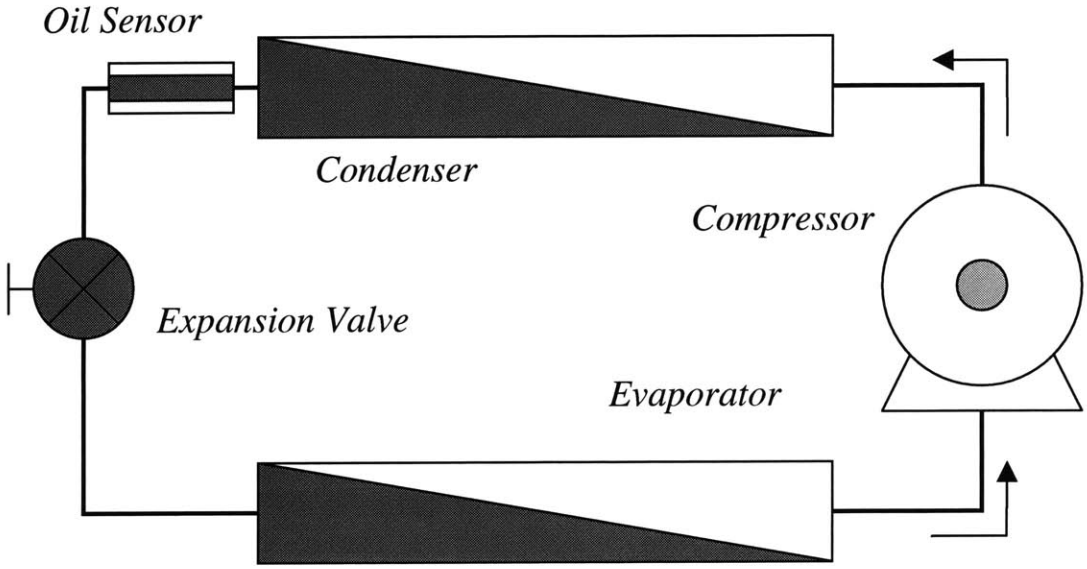

Figure 26: A generic HVAC circuit with the addition of an oil concentration sensor at the outlet of the condenser. The sensor measures the OCR at this point in the cycle.

Although the condenser outlet is the best location for total fluid samples, when the air conditioner is not operating at sub-cooled conditions, gas bubbles can be seen flying through the jet stream in the quartz windows.

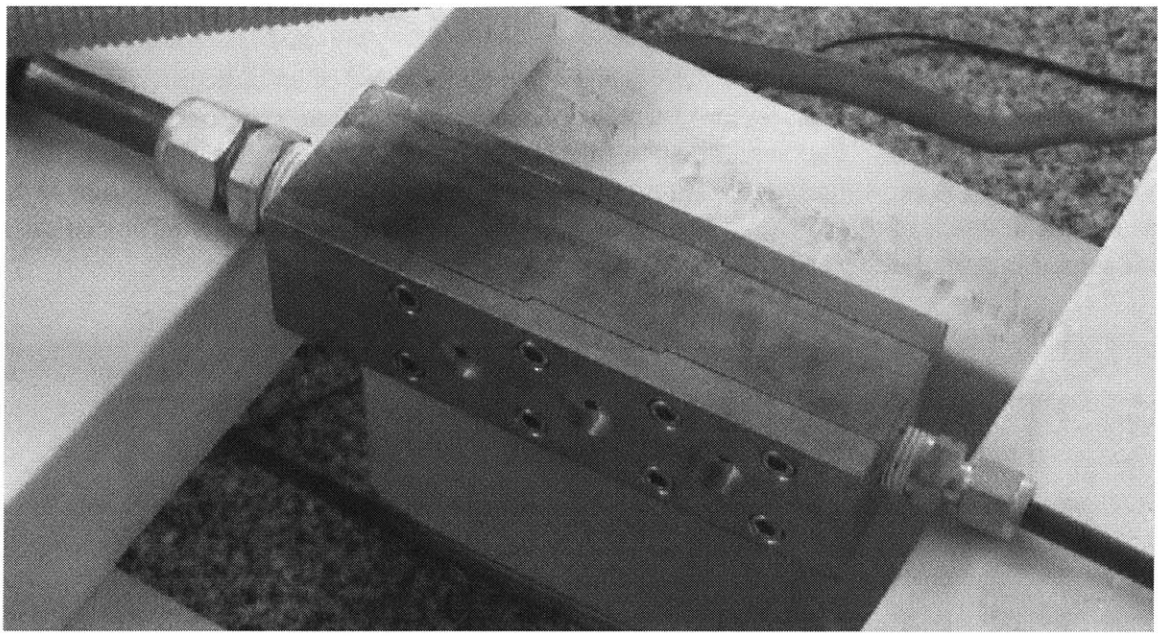

Figure 27: An image of the vessel installed in the HVAC unit. Tubing from the condenser was cut and rerouted out of the air conditioner packaging to give the oil sensor access.

A high volume flow rate of bubbles can corrupt the sensor measurements – the flow of bubbles causes noisy spikes in the absorbance measurements. Vapors actually have low extinction coefficients; so the jump in absorbance is likely due to the interface between the gas and the liquid. As a result, the bubbles must be separated from the flow that passes through the sensor for reliable readings. A simple solution to this problem that does not require complicated geometries or specialized parts will be shown.

Typical operating conditions for this device at this stage of the cycle are the following:

- Temperature: 45 °C
- Pressure: 2.5 MPa
- Flow rate 1 m/s

7.3.1 Optical switching

Because there is only one spectrophotometer and three pathlengths, the optical path from the instrument to the fluid sample must be switched N-1 times for each measurement. Taking all the measurements simultaneously is preferable – this way changes in the time varying system will not appear as nonlinearities in the absorbance measurements. But this would require more sensors, and each sensor may require a separate calibration. One advantage of using a single photometer is that a constant baseline absorbance is guaranteed. An optical network with one spectrophotometer could look like the diagram below; the black lines represent fiber optic cables.

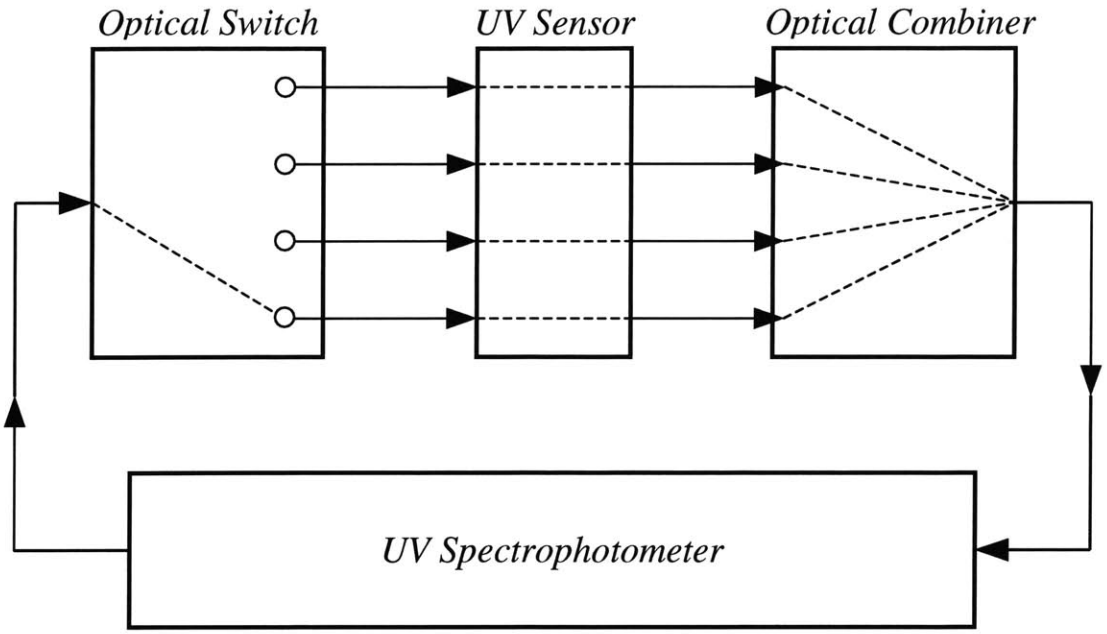

Figure 28: A diagram of an ideal optical switching network for a device with many pathlengths. Currently the sensor uses one set of fiber optics and probes that are manually repositioned during the measurements.

Automated optical switches like the one in the diagram are usually made with accurately controlled mirrors. However, the optimal UV wavelength range used in this sensor does not have many commercial applications. As a result, optical switches with a suitable range are not affordable. Because a suitable switch could not be found, the switching was performed manually by relocating the probe tips to the optical port for each measurement. The repeatability of this switching is acceptable, as it causes less variation than the current calibration technique (±5% reading). The image below shows the alignment module that ensures the probe tips are parallel. The tips slide easily through the module into the locating pockets on the vessel's face.

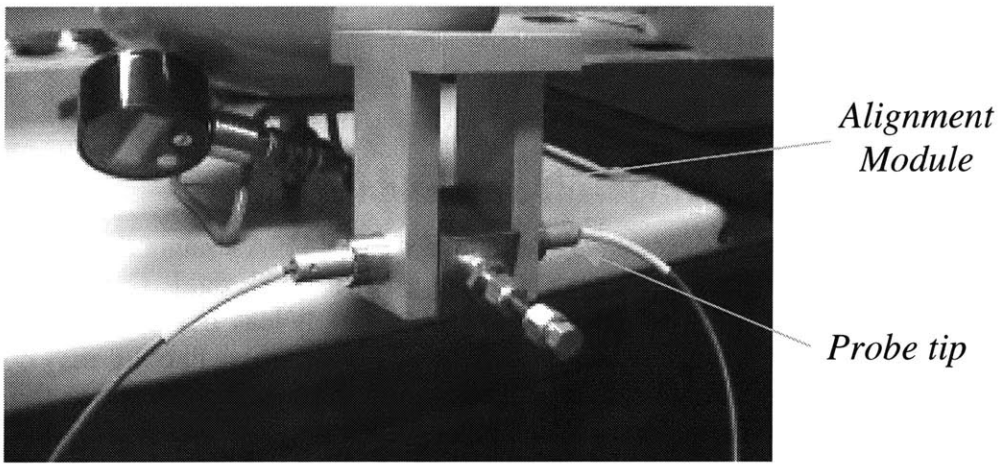

Figure 29: An image of the alignment module placed over the sensor. The module is critical to ensure the repeatable and low absorbance alignment of the probe tips.

7.3.2 Parallel fluid network

The original sensor was installed in series with the air conditioner tubing. This meant that the fluid had to pass through a few more bends and ducts, creating a larger pressure drop in the system. This is a small concern, however, because the pressure drop through the sensor network is expected to be extremely small relative to the entire system. The second sensor was installed in a parallel fashion, shown below.

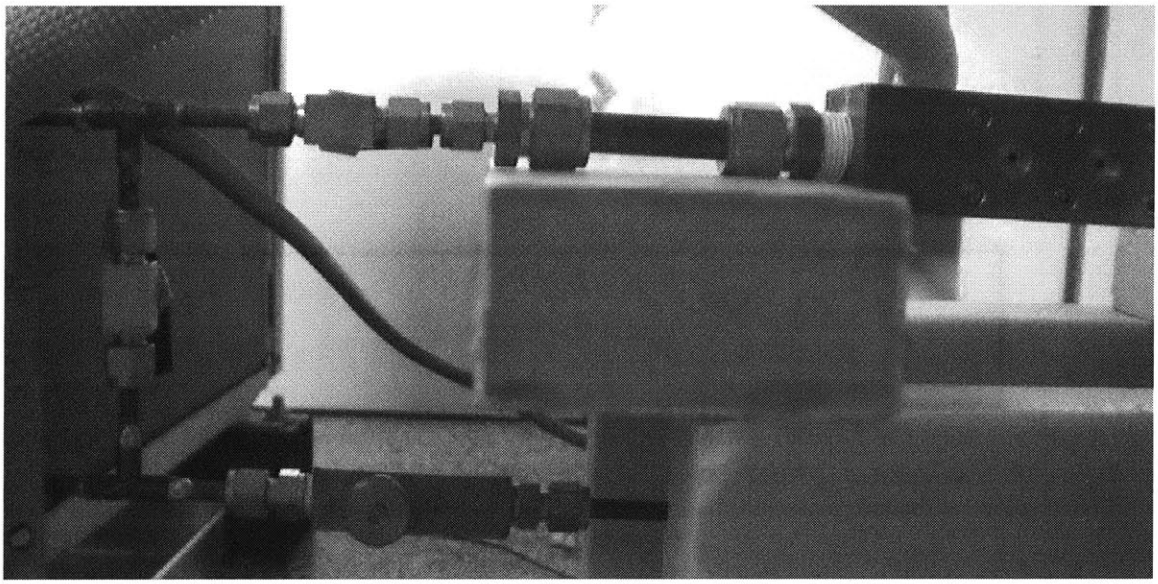

Figure 30: An image of the parallel fluid network extending from the condenser. Two ball valves and a metering valve give total control of the percentage of flow through the sensor.

The valves in the parallel network give the operator control of what percentage of the total mass flow rate pass through the sensor. Closing the valves about the sensor will stop all flow through it and trap a sample. This allows the user to make time delayed (due to manual switching) measurements of a dynamic sample. Furthermore, slowing or stopping the flow rate can often increase the pressure just enough to remove bubbles in the sensor. This configuration also reduces the total pressure drop of the system.

8 Testing and results

8.1 Offline Calibration

8.1.1 The pure refrigerant calibration

The pure refrigerant was calibrated using R410A straight from the gas tank. The sensor was connected to the tank and allowed to fill with fluid. Figure (29) shows a picture of the setup. The vessel has to be completely leak free because any leaks cause spontaneous bubble formation in the fluid. Although these bubbles may not be visible to the eye, they can severely contaminate the data. The plot below shows three measurements of absorbance for the three pathlengths of the sensor.

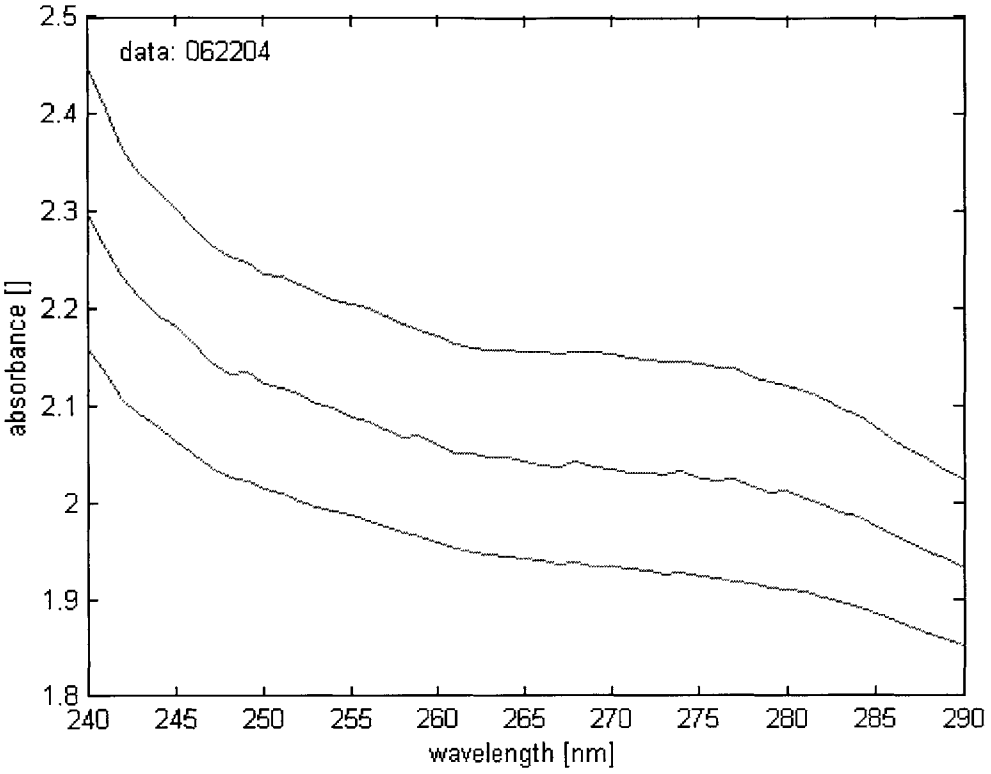

Figure 31: A plot of R410A absorbance versus wavelength for the three pathlengths in the sensor.

The next plot shows how linear this data is at 264 nanometers. This is an indication that the procedure was done correctly and the data fits the model well.

The final plot shows R410A's extinction coefficients estimated from the data above. These data were taken at room temperature, which is about 20°C cooler than in the inline configuration.

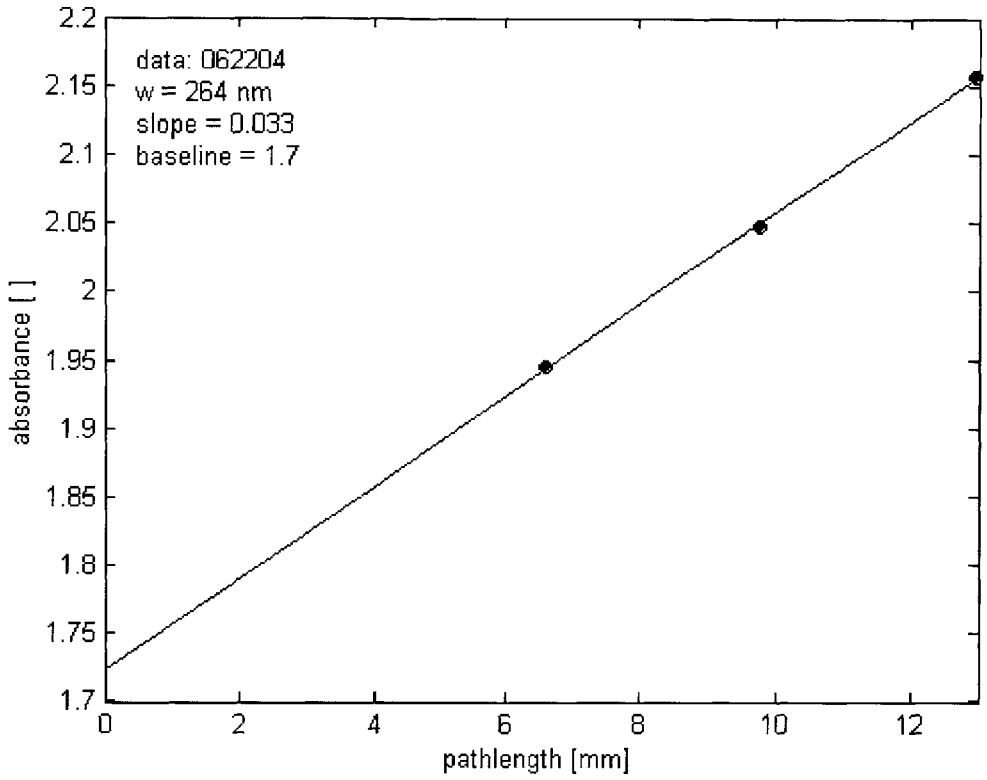

Figure 32: A plot of absorbance versus pathlength linearity at 264 nanometers.

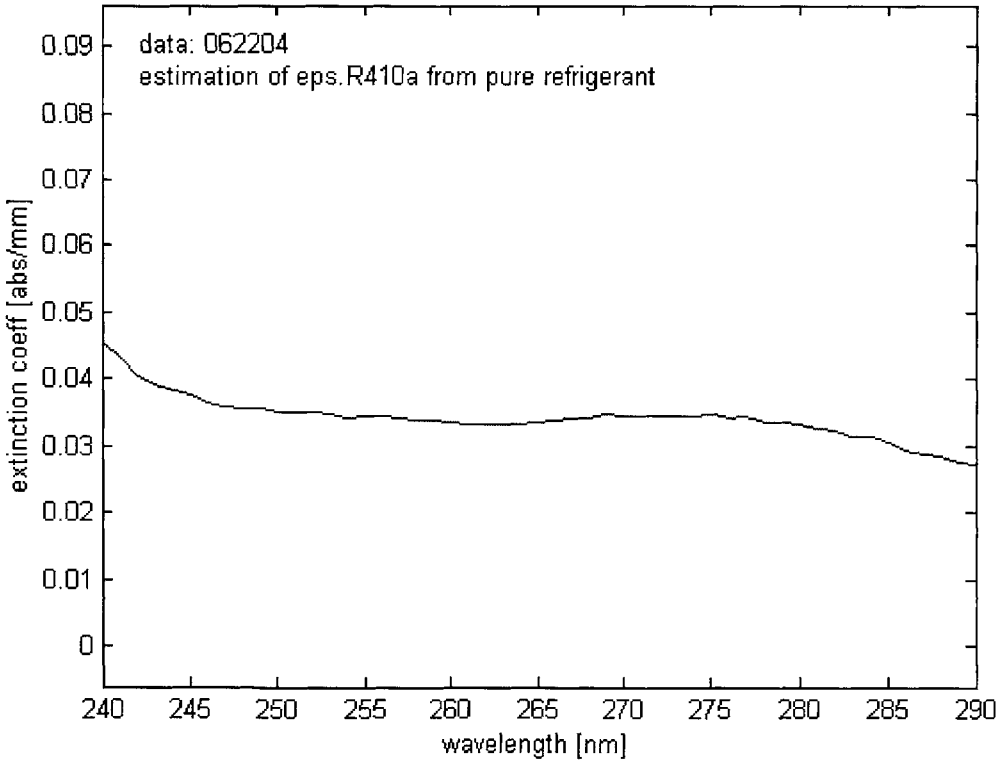

Figure 33: A plot of the estimated extinction coefficients reduced from the data above.

8.1.2 The mixed sample oil calibration

The oil calibration requires careful sample preparation. The accuracy of the sensor depends heavily on the ability to calibrate its absorbance measurements with known oil concentrations. Because the R410A can only be handled in enclosed vessels at room temperature, it is not amenable to these measurements. Therefore, isopropyl alcohol was used as a substitute refrigerant to dilute the oil.

The mass of the two fluids were measured and mixed thoroughly in a beaker. The weight concentration was then converted to a volume concentration for use in the calibration techniques. The image below shows a scale and beaker used for these measurements.

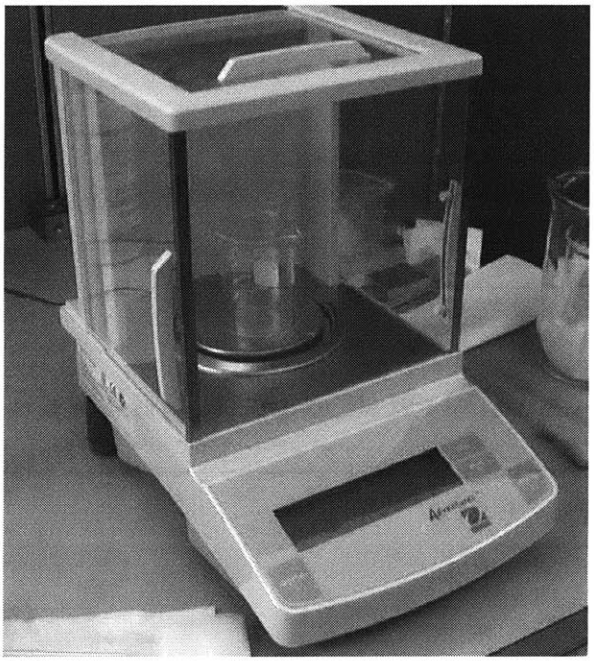

Figure 34: An image of the high accuracy scale used for calibration measurements.

The plot below shows five samples that were taken at three pathlengths. Oil volume concentrations of 0.00, 0.52, 0.76, 0.92, and 1.29 percent were measured at 6.59, 9.77, and 12.94 millimeters over a wavelength range from 200 to 350 nanometers. Five concentrations, three pathlengths, and 150 wavelengths were acquired in a total of 2250 absorbance measurements.

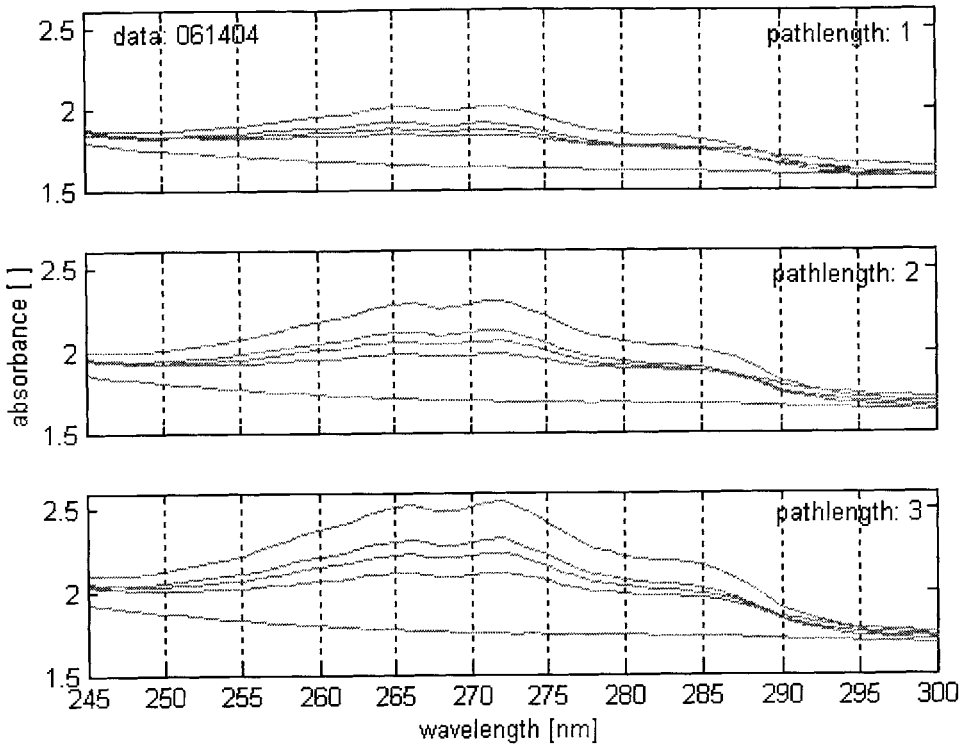

Figure 35: absorbance data for FVC50k oil in isopropyl alcohol, between 0 to 1.29% oil

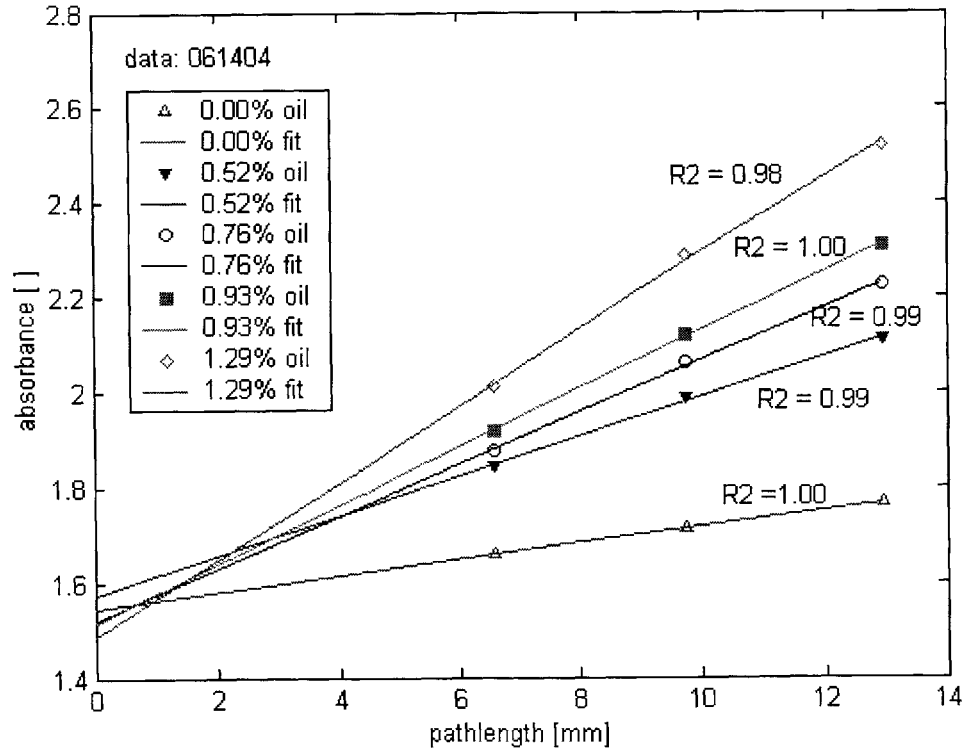

Figure 36: Absorbance data shows good linearity with pathlength. Each concentration line comes to a similar estimation of the baseline absorbance at "zero pathlength"

The plot above shows the absorbance versus pathlength linearity for each of the five concentrations. All the linear fits are good and have R^2 values above 0.98, but they should also agree on the baseline absorbance. The baseline absorbance at zero pathlength in this plot has an uncertainty less than ± 0.1 absorbance. This waws typical of the data.

The next plot is the estimated extinction coefficients for the oil FVC50k and the isopropyl alcohol. Three methods are shown in the plot below: a least squares minimization of the linear regression from Equation (48), a differential calculation from Equation (14), and a similar calculation that subtracts the baseline absorbance based on Equation (11). The latter two methods do not take into account the absorbance due to refrigerant, so their predictions of the oil extinction coefficients result in much higher absorbance rates.

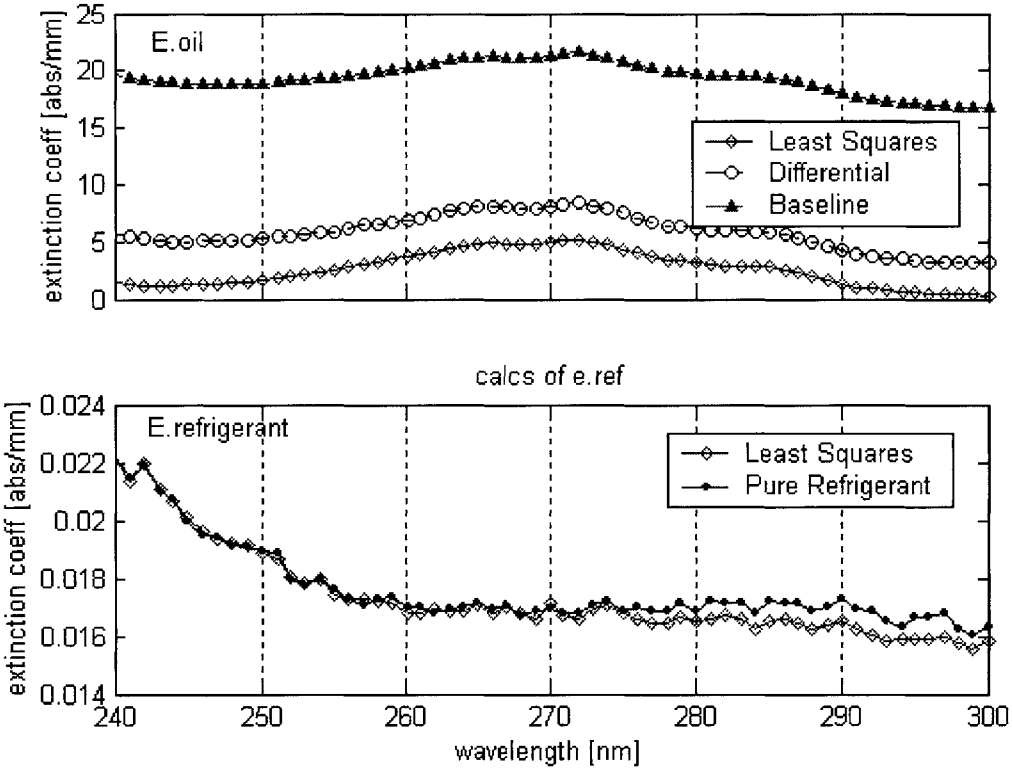

Figure 37: An estimation of the oil (upper) and isopropyl (lower) extinction coefficients. Three methods are compared for the oil coefficients. The juxtaposition shows the overestimation oil absorbance rates in methods that do not account for the refrigerant.

To test the calibration quality, multiple samples of a 1% oil concentration sample were prepared. The concentrations were measured on the scale as 0.98, 1.02, 1.03, and 1.04 oil percent. The plot below shows the signal to noise ratio for each pathlength. The noise was estimated by the standard deviation of the individual wavelength data. A ratio of 100:1 is good considering the oil concentrations themselves were known to be in variation of at least that much. This signal to noise measurement shows that entire calibration procedure from sample preparation to manually switching the optical probe tips can be controlled to approximately 1% uncertainty on absorbance measurements.

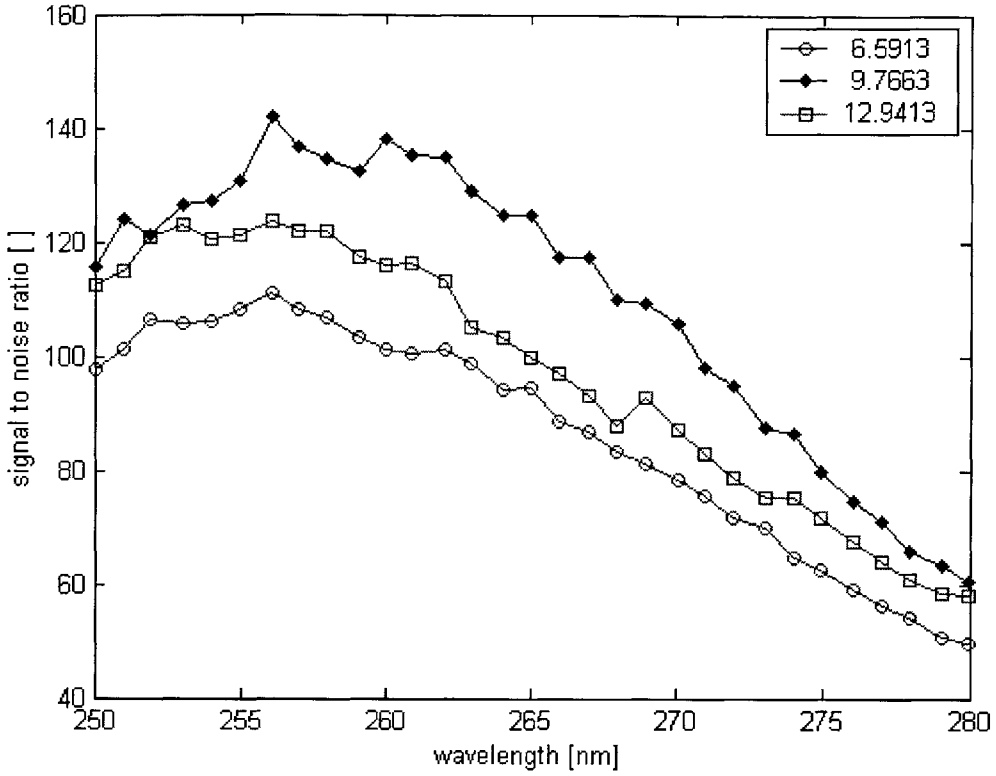

Figure 38: A plot of signal to noise ratio for repeated 1% oil concentrations. Noise is taken to be the standard deviation of the data.

8.2 Inline testing

The sensor calibrated with above data can readily be used to make measurements of the OCR at the outlet of the condenser. Although the calibration was not performed at the ideal conditions, for the purposes of this report the room temperature calibration is assumed to be acceptable. The pressure and temperature calibration from the Jasco product [4] showed a very low dependence.

The plot below shows various scans of inline data at three pathlengths. The sensor typically reads near zero percent oil at regular operating conditions. To heighten the OCR, the compressor was run at a high frequency and the ambient air temperature of the outdoor unit was allowed to heat up. Under such conditions, superheated vapor is more likely to pass through the compressor and bring more oil with it. At a compressor speed of 80 Hz and an air temperature of 35 °C the oil becomes visible to the eye. As shown in the line with red circles in the plot below, the signature shape of oil's absorbance spectra can be seen under these conditions. The two peaks are subtle, but they can be seen at the usual locations of 266 and 272 nanometers.

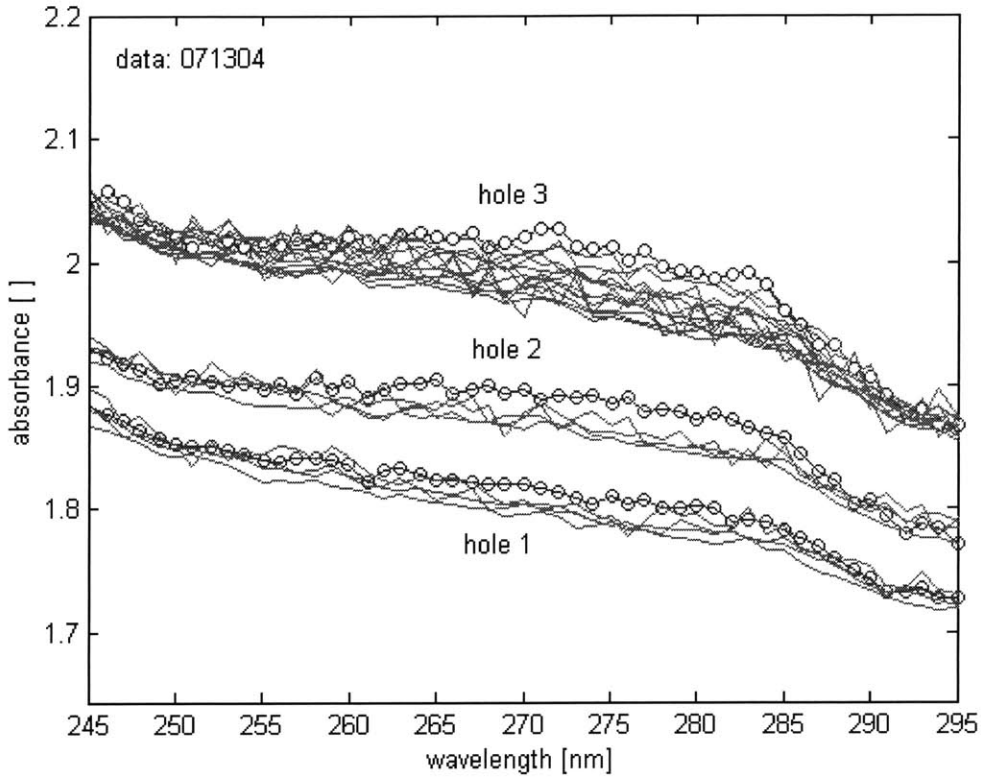

Figure 39: A plot showing the three pathlength data from the inline sensor. The three scans shown in red circles is a set of data with the strongest sign of oil.

Note that the other data is very noisy. This noise is an example of the data taken when the condenser is not sub-cooled and the valves are left open. The valves were left fully open during this test to increase the chance of oil passing through the sensor. This noise was handily reduced when the valves about the sensor were closed, stopping the flow of bubble interfaces through the optical path. The data highlighted is much cleaner than the data when the valves were left fully open.

After all the data was taken, it was analyzed offline and estimates of the oil concentration were made. The bar plot below shows the estimates of the peak oil data for various methods. At around 0.5% oil – the center of the operating range of the sensor – these methods tend to generate similar oil concentration measurements.

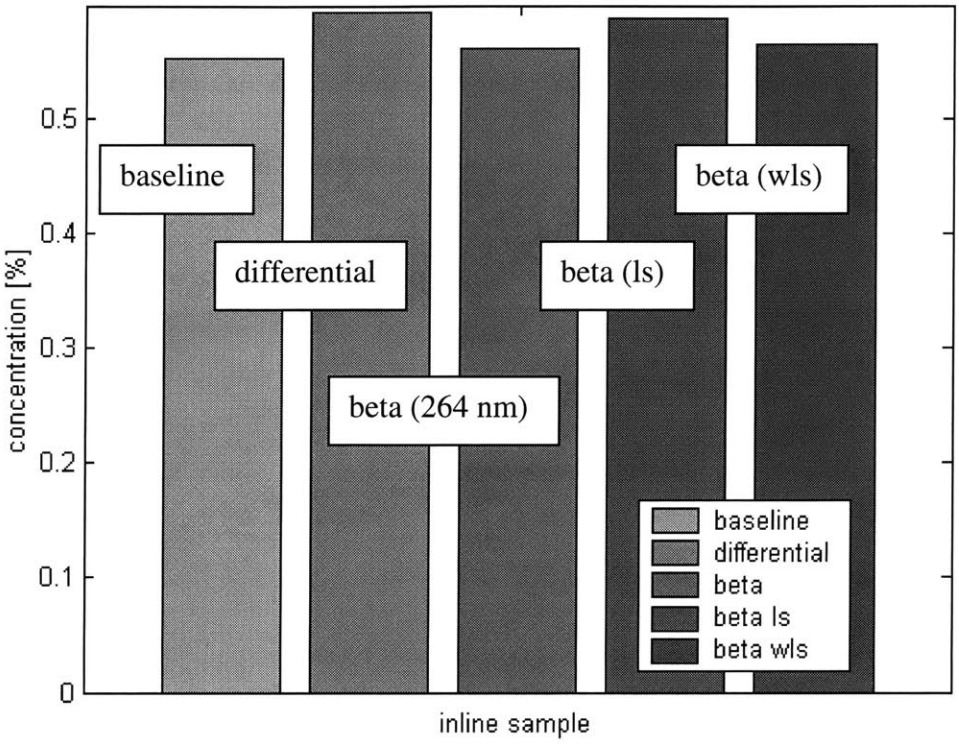

Figure 40: A bar plot of various techniques' estimates of the oil concentration found in the inline data. The three methods on the right are base off of linear regression.

8.3 Performance comparison of various techniques

The best indication of the sensor's accuracy is found when a calibrated sensor is used to measure samples of known concentrations. This test shows how repeatable and accurate the data gathering process is and how robust the various analysis techniques are to noise in the data.

The extinction coefficients have already been shown for the least squares, baseline, and differential methods of analysis. Now these three techniques will be used to measure the known samples. To be consistent, each technique uses the same assumptions and equations it did during calibration.

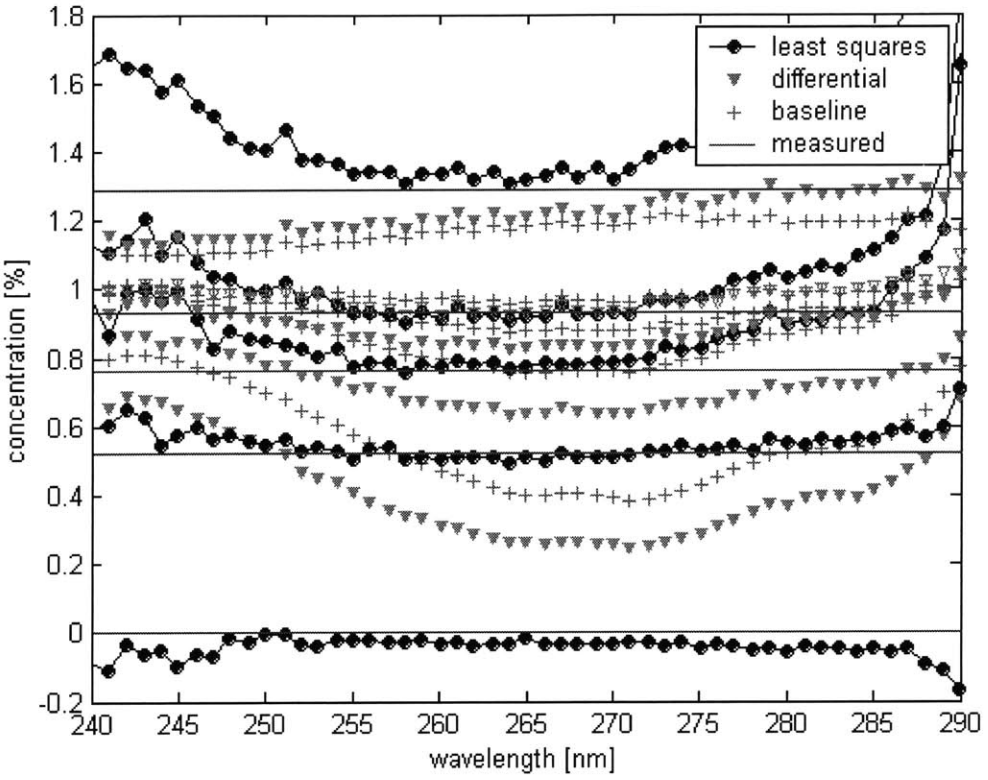

Figure 41: Results from five known samples are shown above. Plots are of the various techniques' predictions against wavelength. The red lines are the measured standard, and the black circles are the predictions from linear regression.

The plot above is difficult to view at a glance. However, one observation stands out: at oil concentrations below 0.5%, the differential and baseline methods cannot track the measured value. Indeed the least squares method (black circles) is very similar to the differential method (down-facing triangles). The least squares "beta" method currently only uses one extra pathlength of information. The inclusion of the refrigerant in the model is what enhances its performance at these concentrations.

Looking at each wavelength's prediction is also important when attempting to choose the optimal wavelength or a weighting matrix. The predictions made at each wavelength are coordinated together through least squares and weighted least squares techniques presented in Equations (55) and (60), respectively. These techniques generate an overall estimate based on all of the estimates above. The plot below shows the performance of these techniques as well as the other techniques at the optimal wavelength (263 nanometers).

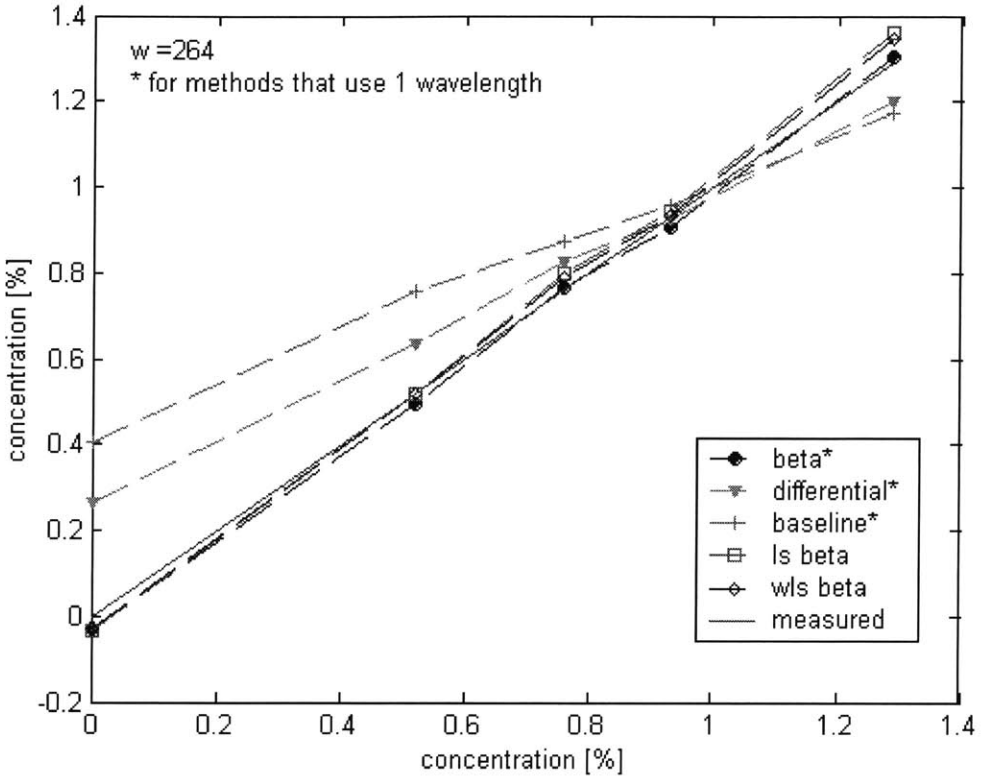

Figure 42: A plot of various techniques' estimates against measured concentration. The red line is the measured value, and the three lines that follow it closely are all based off of linear regression techniques.

The plot above clearly compares each method's ability to track the known sample's concentration. Most notable is the growing discrepancy with lowered oil concentration for the methods that do not account for the refrigerant. Another way to look at this plot is the error from the measured value. The error is simply defined as the following

$$error = \frac{\hat{c} - c_{measured}}{c_{measured}}. \tag{61}$$

Therefore, the error is undefined at an oil concentration of zero. The decreasing oil concentration, $c_{measured}$, adds to the increasing error that the differential and baseline techniques demonstrate in the plot below. At an OCR of 0.5% the errors of these techniques have already grown to 20 and 50 percent. The other techniques are basically within ±5 percent error. Consider that ±5% on a reading of 0.5% is an uncertainty of only 0.025% on oil concentration. This greatly exceeds the expectations of the UV method as posed by United Technologies Research Center [2].

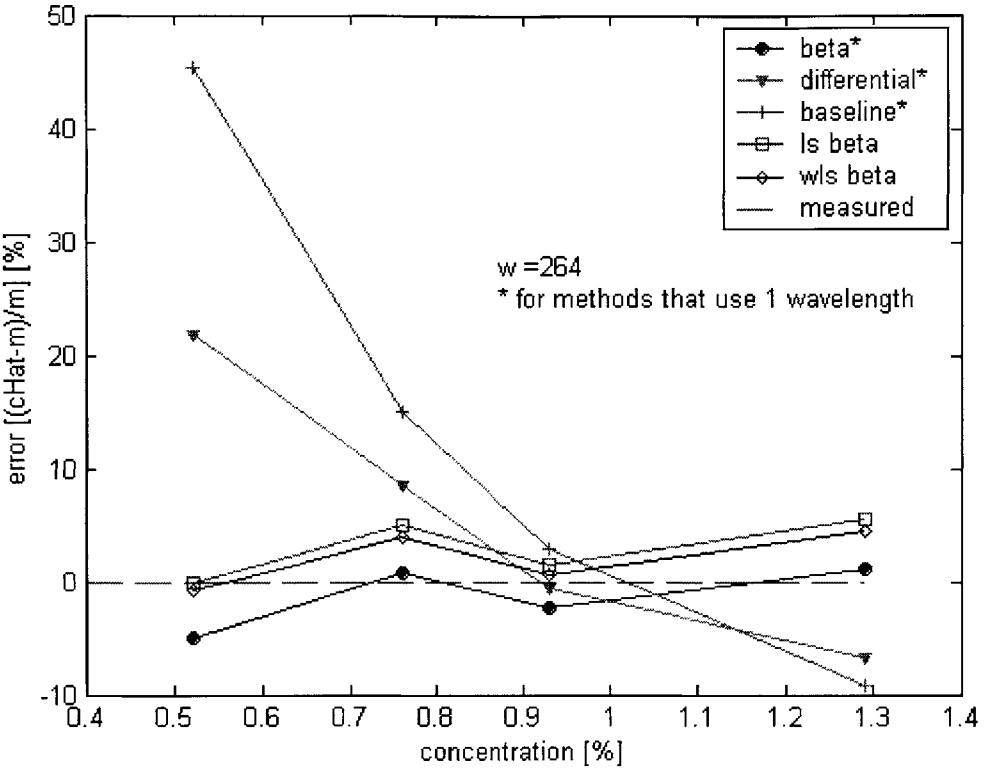

Figure 43: A plot of various techniques' error against measured concentration. The red line is the zero error line, and the three lines that follow it closely are all based on beta techniques.

The plot below is a zoomed-in version of the plot above. The three techniques that are based on the linear regression can be evaluated more closely. The weighted least squares method (black diamonds) performs the best in this test. As a result, that is the suggested method to use over the operating range of the device.

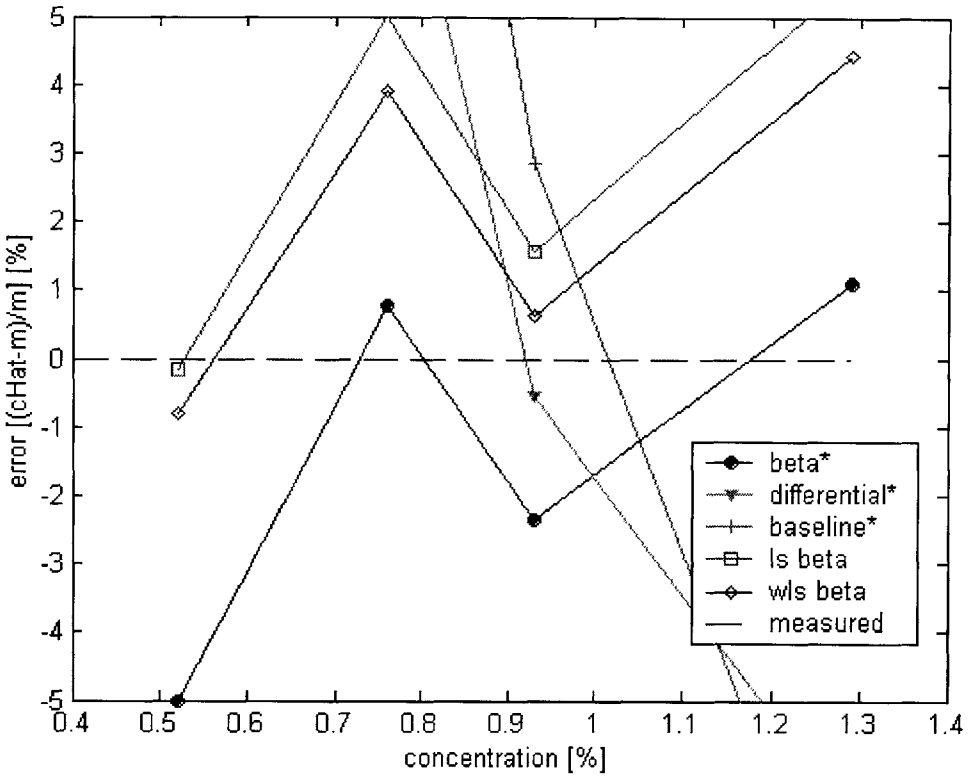

Figure 44: A close-up plot of the estimation error. The weighted least squares (black diamond) technique based on linear regression is shown to be the only technique within ±5%.

9 Conclusions

A number of conclusions can be drawn from the performance comparison shown above. As mentioned, the most significant result is that the inclusion of the refrigerant in the model can increase the operating range of the sensor down to zero percent oil concentration. The linear regression technique does not show any preference to high or low oil concentrations like the other techniques.

An interesting observation can be drawn from the plot showing each wavelength's estimation. This plot is arguably the best way to define the optimal wavelength: the less the error from the measured value, the better the wavelength. This calculation was performed and the result is shown below:

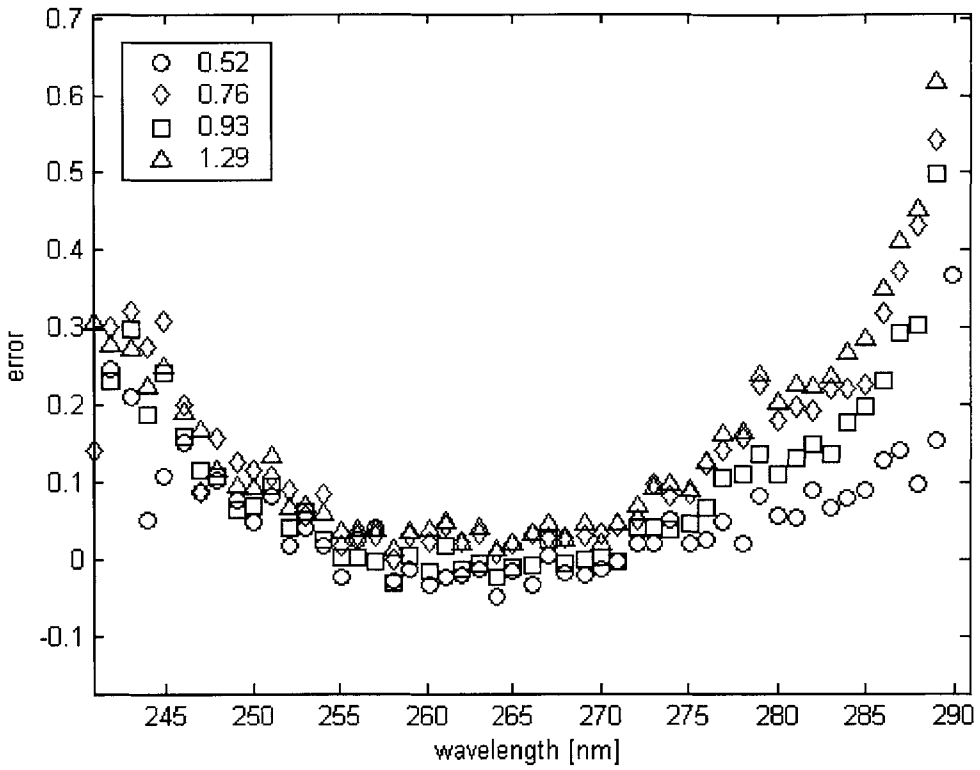

Figure 45: A plot using error in the estimation as an indicator of the optimal wavelength. A calculation of error is made for each known sample at each wavelength. The error clearly depends on wavelength and do not appear to be heavily correlated to the sample concentrations.

This result corroborates the calculation of the optimal wavelength based on linearity with concentration and pathlength. For comparison, the weighting from this metric was presented in Figure 17. They both indicate a clear point at 263 nanometers with the lowest error.

It was not expected to find one wavelength that was so clearly dominant and reliable for concentration estimation. This raises the question as to whether or not the sub-optimal wavelengths should be used at all. Reducing measurement noise through redundant data can still be achieved by taking multiple measurements at the optimal wavelength.

The sensor has been designed, implemented, installed, calibrated, and used to measure the dynamic OCR in an HVAC unit. The beta method and its variant using the weighted least squares is suggested as the best analysis technique to reduce the data. However, some experimentation with the current wavelengths and weighting factors may be found to enhance the estimations over a broader range of training data.

10 References

1. Hyun Jin Kim, Timothy W. Lancey, *Numerical study on the lubrication oil distribution in a refrigeration rotary compressor*, February 5, 2003
2. United Technologies Research Center, *Study of Lubricant Circulation in HVAC Systems*, October 1996
3. Richard Brereton, *Chemometrics: data analysis for the laboratory and chemical plant*, 2003
4. Wada, M. Nomura, and K. Tsuboi, Jasco Corporation and K. Kutsuna and T. Nabeta Nippondenso Company, *A Novel Approach to Instrumentation and Application for OCR Measurement in Refrigeration System*
5. John A. Rice, Mathematical Statistics and Data Analysis, Second Edition, 1995
6. Paul M. DeRusso, Rob J. Roy, Charles M. Close, Alan A. Desrochers, State Variables for Engineers